Lessons learned using empirical methods applied in mining

N.R.Barton
Nick Barton & Associates, Oslo, Norway

ABSTRACT: This paper is designed as a broad-brush resume of some methods developed by the writer, which have also found application in mining, even though the focus of the original developments was from civil engineering. Methods summarized will include estimation of shear strength for rock cuttings and benches, with possible application to open-pit slopes. Emphasis will be on the estimation of shear strength-displacement and dilation-displacement for rock joints, with allowance for block size. Rock dump stability assessment will also be touched on. Some adverse practices will be mentioned concerning direct shear testing. Estimation of the shear strength of rock masses will be included in the discussion. This will lead into the Q-system parameters, and how they can assist in shear strength estimation if one is forced by the scale of problem to perform continuum analyses. The Q-system's six parameters can assist in selection of support for permanent mine roadways and shafts. The six Q-parameters are also useful for statistical rock quality zonation of future mining prospects, based sometimes on the characterization of hundreds of kilometers of drill-core. The Q-system's first four parameters have been widely used in mining for stope categorization: stable, transitional, caving, and assessing the need for cable reinforcement. Some parallels between unsupported excavations in civil engineering and in mining engineering will be drawn, with emphasis on ESR, the modifier of span.

1 INTRODUCTION

1.1 *Shear strength of intact rock*

Although many still use linear Mohr-Coulomb, or non-linear Hoek-Brown, it is easily demonstrated that these will introduce inaccuracy if stress ranges are large. A new non-linear criterion, based on an old idea (critical state) has recently been developed, showing correct deviation from Mohr-Coulomb. A few tests at low confining pressures define the whole curved envelope. The critical confining pressure required for (weaker) rocks to reach maximum strength, where the strength envelope becomes horizontal, is found to be close to the uniaxial strength of the rock (Singh et al. 2011, Barton, 1976).

1.2 *Shear strength of jointed rock*

Here it is also found that many still use linear Mohr-Coulomb. Over a limited stress range, and with more planar joints this is defensible. Part of the reason for continued use of a nevertheless uncertain *cohesion intercept* is that multi-stage testing accentuates the apparent cohesion. Shear testing the same joint sample at successively increasing normal stress causes a potential clock-wise rotation of the strength envelope. The preferred method is based on index tests for JRC, using tilt tests (not subjective roughness profile matching), and Schmidt hammer tests for joint wall strength JCS. Scale effects caused by increasing block-size are allowed for using empiricism, not *a priori* assumptions. A useful check of the large-scale JRC is the 'a/L' method, measuring amplitude of roughness between straight-edge contact points, provided joint surfaces are well exposed by over-break, for instance in a bench-face

1.3 *Shear strength of rock masses*

Linear Mohr-Coulomb is still popular despite the existence of the also *a priori* GSI-based, modified Hoek-Brown criterion. A potential problem with these standard methods, in addition to the actually complex, process-and-strain-dependent reality, is that some failure of intact rock ('bridges') may be involved. This genuine cohesive strength is broken at smaller strain than the new fracture surfaces are mobilized. These new surfaces have high JRC and JCS and φ_b. The surrounding joint sets, with lower JRC, JCS and φ_r, may get their peak strength mobilized at still larger strain, followed by eventual clay-filled discontinuities or fault zones, if these are also involved. Since this is a process-and-strain related property, and also non-linear, why are we adding c +

σ_n tan φ, and not degrading/mobilizing as in the form 'c *then* σ_n tan φ'? Numerical modelling in Canada, Sweden and India, with FLAC, Phase 2 and FLAC3D respectively, have indicated more realistic results using the 'then' method. Müller (1966) suggested the early degradation of cohesion and reliance on the remaining friction, long ago.

1.4 *Shear strength of rock dumps*

A similar non-linear peak shear strength criterion as the Barton-Bandis crierion for rock joints, can also be used for rock dumps, using parameters R, S and φ_b in place of JRC, JCS and φ_r. It is also practical to perform tilt tests to back-calculate R, and by using e.g. 5m x 2m x 2 m tilt-test boxes, full-scale particle grading can be incorporated. These realistically large 'samples' can be compacted if desired, by building the tilt-test box into the compacted layer, and then excavating it so it is free of the surroundings. This has been done in practice in rockfill dam construction. It works.

1.5 *Shear strength from Q-parameters*

A big case-record data base was used when choosing the Q-parameters, and when developing suitable ratings for the final six parameters. This provided rock mass descriptors in the form of relative block size (RQD/Jn) and friction coefficient (Jr/Ja). This allowed one to differentiate shotcreting needs (due to small block-size and low cohesive strength) from bolting needs (due to low inter-block shear strength). Since the Barton (1995) inclusion of UCS with Q_c = Q x σ_c/100, feasible-looking values of cohesion (CC) and friction (FC) suggested in Barton (2002) can be derived from separate halves of Q_c. As demonstrated by Pandey and Barton (2011), these Q-parameter based versions of cohesion and friction also need to be respectively degraded and mobilized.

1.6 *Q-histogram statistics for ore-body zonation*

EXCEL spread-sheets by-the-kilometer can be generated in order to record the results of tens or hundreds of kilometers of core-logged Q-values and Q-parameters. However, more sense of future mine-zonation exercises is made when histograms of the Q-parameters are plotted. Expect to be pleasantly surprised when tens of thousands of RQD measurements are plotted for the central Q = 1 to 4 rock mass class. Those criticising RQD need to be silent.

1.7 Q-*system for roadways and shafts*

The original B+S(mr) reinforcement and support recommendations from Barton et al. (1974) were replaced by B+S(fr) in the update of Grimstad and Barton (1993). These single-shell methods have been used successfully in countless thousands of kilometers of tunnels for hydropower, for road and rail, and especially for mine-roadways. B + S(fr) is also used in thousands of caverns, including three 30m span 'road turning caverns' at 1000 to 1400 m depth along the 24.5 km long Lærdal road tunnel in Norway. A suggested Q-based approach to shaft reinforcement and support is to put diameter as the height dimension in the Q-system. The validity of '5Q and 1.5ESR' for temporary support in civil engineering tunnels and caverns awaiting a final (double-shell) concrete lining is confirmed by practice.

1.7 *Stope stability using Q'*

Since the early eighties, the first four Q-parameters, generally termed Q' (or N) have been used in the mining industry ('modified Matthews' etc.) for helping to dimension or categorize stopes (stable, transition, dilution, caving) for ore-body exploitation. The writer has noted the need for a stress/strength substitute for SRF, and the apparent need of a faulted rock term, and for rock affected by the nearby presence of a fault. Maybe the dissection of Q was premature.

1.9 *ESR parallels from civil and mining*

A graphic presentation of the 'operator' ESR is needed in order to see where the different categories of mining stopes (stable, transition, caving) actually lie in relation to ESR values. This is done for various excavation dimensions.

2 SHEAR STRENGTH OF INTACT ROCK

A long time ago, following observation of the actual curvature of triaxial strength data for intact rock, the writer (Barton, 1976) proposed the definition and quantification of a critical state for intact rock (shown in Figure 1), whereby the 'final' (pre-cap) horizontal condition of a given strength envelope could be utilized. Going unnoticed for several decades, this concept has recently been used by Singh et al., (2011) to quantify the necessary deviation from linear Mohr-Coulomb.

The two most elegant factors about the Singh et al., (2011) criterion is that fewer in number, and only low confining stress triaxial tests need be performed, in order to define the whole strength envelope. Furthermore, the critical confining pressure for most rocks tends to be equal or nearly equal to the relevant UCS value, as indeed depicted in Figure 1 (see circles #2 and #4 which are nearly tangent). This is an almost logical and elegant finding.

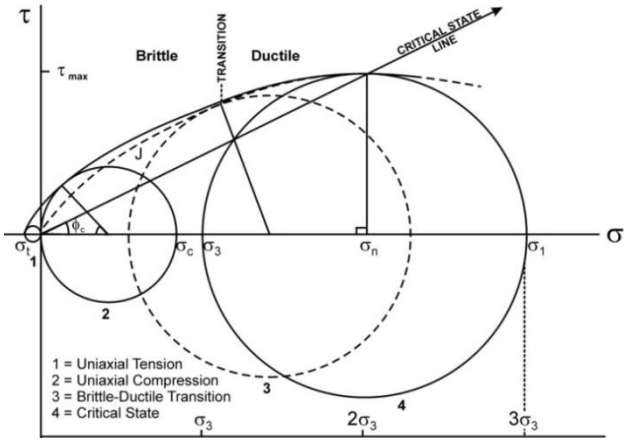

Figure 1. Brittle-ductile transition and critical state for rock. The curvature is ignored in the petroleum industry. We should not make the same mistake in civil and mining. Barton, 1976.

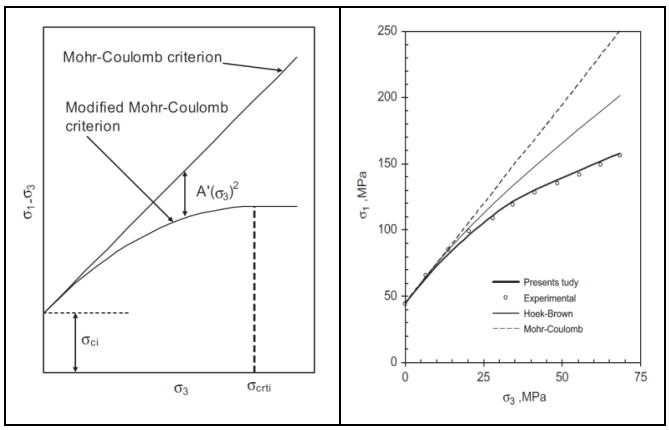

Figure 2. The Singh et al., (2011) approach to improving the description of shear strength, by quantifying the necessary deviation from Mohr-Coulomb. Note the greater curvature than the intact-rock Hoek-Brown criterion.

3 SHEAR STRENGTH OF JOINTED ROCK

There are countless applications for the shear strength of rock joints in both civil and mining (and petroleum engineering). Nevertheless, there are some strange testing practices being used and recommended by some consultants. Among the strange practices is the performance of multi-stage testing. (Are jointed core samples really so rare?). This practice may accentuate the (apparent) cohesion, because clock-wise rotation of the strength envelope 'fitting' the typical four tests may occur. Imagine a lower strength rock and a rougher rock joint. Damage is inevitable. A third strange practice is the subtraction of the dilation from the peak strength. This seldom cited but 'popular' method ignores the asperity failure component S_A which is illustrated in Figures 3 and 4, from Barton (1973) and Bandis et al. (1981). As can be noted in Figure 4, the component S_A operates at all scales. If just the dilation angle is subtracted from the total strength, one is left with an ill-

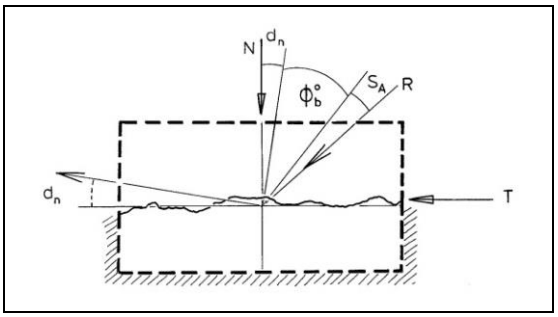

Figure 3. The principal shear strength components of a non-planar, dilating rock joint, from Barton (1971, 1973).

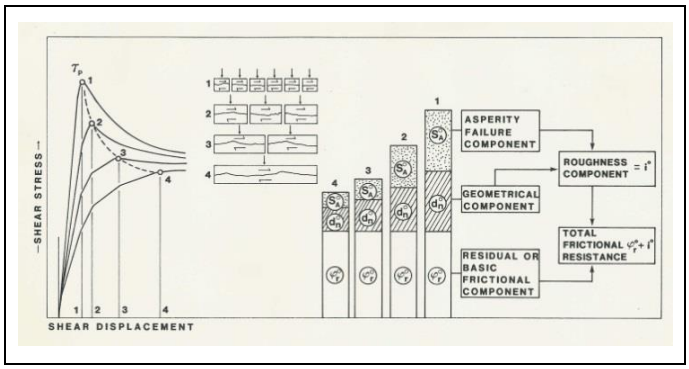

Figure 4. The peak shear strength component S_A is of similar magnitude to the dilation angle. Bandis et al. (1981).

defined 'frictional' component, often as much as 40°, which seems to be a hazardous number onto which to add roughness, as practiced in some Australian mining operations, as far as is understood.

3.1 *Curved envelopes and index tests for joints*

Figure 5 illustrates in conceptual terms, all the potential strength components of a rock mass, starting with the intact 'bridges' and ending with the potentially mobilized filled discontinuities. The new fractures, formed at small strain, have higher shear strength than most rock joints, which mobilize full strength at larger strain. As suggested in the introduction, it makes little sense to add the cohesive (intact 'bridge') strength and the frictional strength. Instead, greater realism is achieved by degrading cohesion while mobilizing frictional strength.

It is interesting to register the confidence of some young recently published researchers who criticize the use of the JRC roughness numbers associated with the profiles given in Figure 7, when the basis of their critique is shear tests on a limited number of artificial replicas of joints. A criterion based on direct shear tests of 130 individual *natural rock joints*, testing only once per sample is inevitably more reliable than they have assumed. Furthermore, the instruction to perform tilt tests to obtain roughness, or at least the 'a/L' (amplitude over length) measurement, seems to be ignored by many, when they attempt to document the subjective nature of profile-matches.

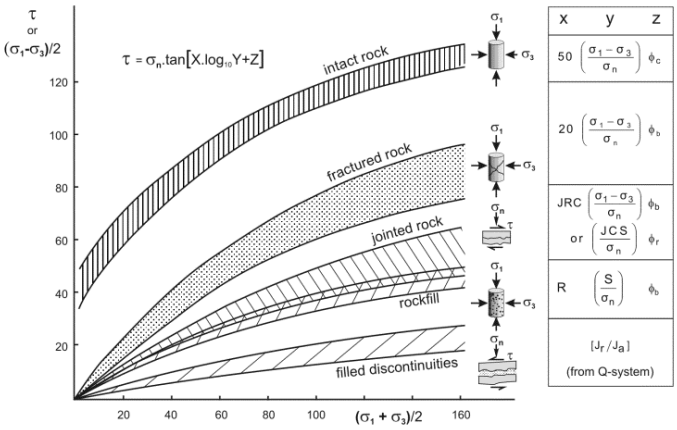

Figure 5 A conceptual (and actual empirically applicable) collection of curved shear strength envelopes and criteria for the three or more components of rock mass strength. Barton, 2006.

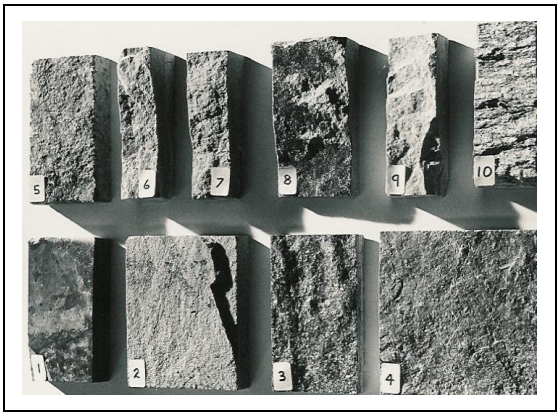

Figure 6. Ten of 130 natural joint samples which lie behind JRC, JCS. Relevant roughness profiles are shown in Figure 7.

It has also been interesting to note the insistence of at least one recently published researcher, using PFC modelling techniques, that the 'order' of the JRC profiles (Figure 7) is partially' incorrect'. Unfortunately his conclusion is itself in error: the profiles shown have JRC_0 (small-scale as shown) within the measured range, and they do apply to the ten tested samples illustrated. Close examination will of course indicate the possibility of anisotropic JRC, such that direct shearing must be in the direction of interest.

As pointed out by Barton and Choubey, 1977, the performance of tilt tests (or gravity-loaded pull-tests) is preferable to profile matching. The tilt test principle, as illustrated in several forms in Figure 8, has been used successfully on countless numbers of core-derived samples (sawn joint-parallel), and even on 1.2 m long and 1.3 tons diagonally-fractured 1 m^3 rock blocks (Bakhtar and Barton, 1984), and also on 5x2x2 meters rockfill samples (Barton, 2013). The non-linear shear strength criterion takes care of extrapolation to stress levels at least four orders of magnitude larger, i.e. through the level needed for benches, up to open-cast design.

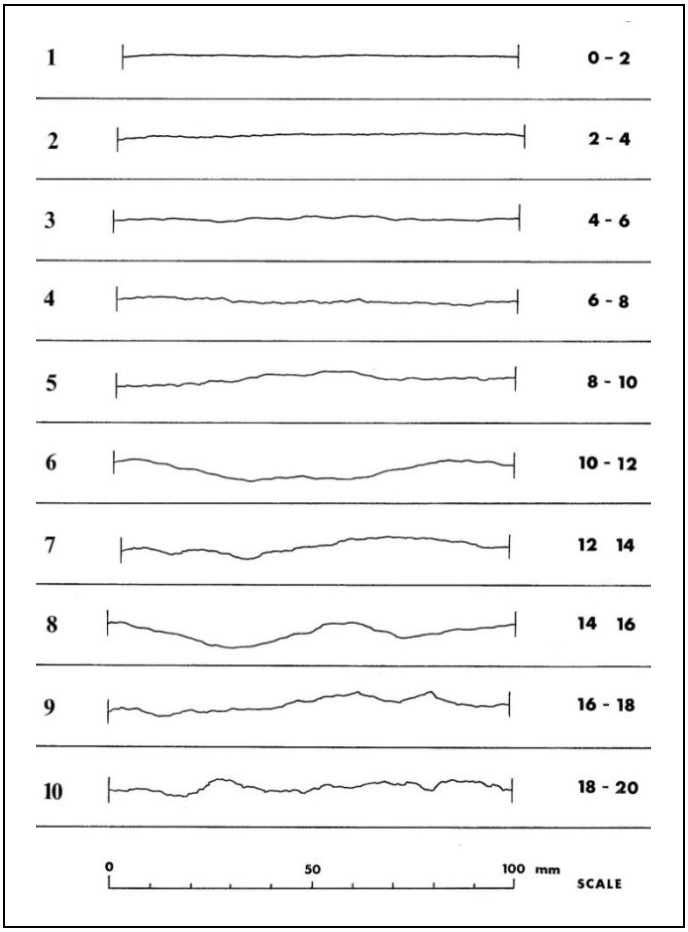

Figure 7. The original ten roughness profiles at 100 mm scale from Barton and Choubey (1977). There are several unreliable reproductions of this in the literature. This is the original set.

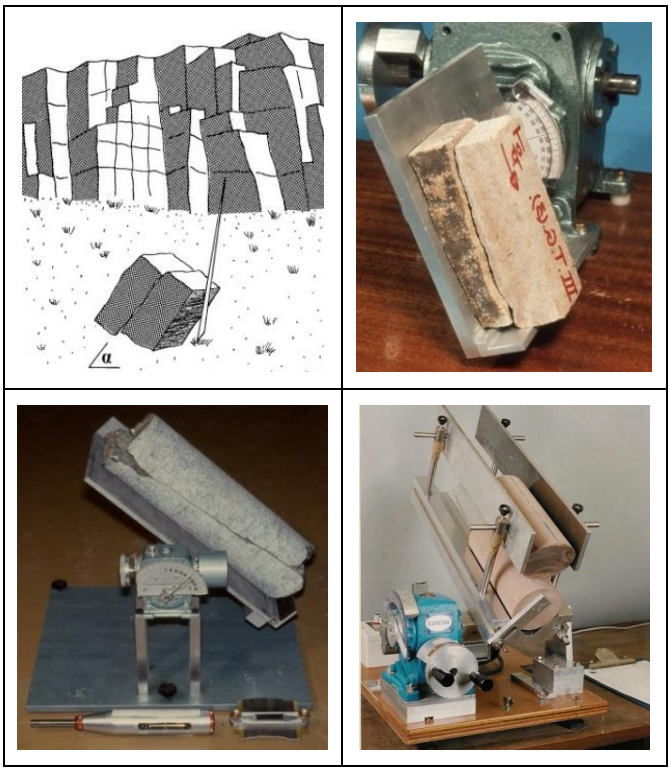

Figure 8. Concept sketch and photographs of three tilt tests using a sawn block (as in 1976 study), a large jointed core (1990's) and twin core pieces in vertical contact (1990's for φ_b). These tests have σ_n as low as 0.001-0.002 MPa at failure.

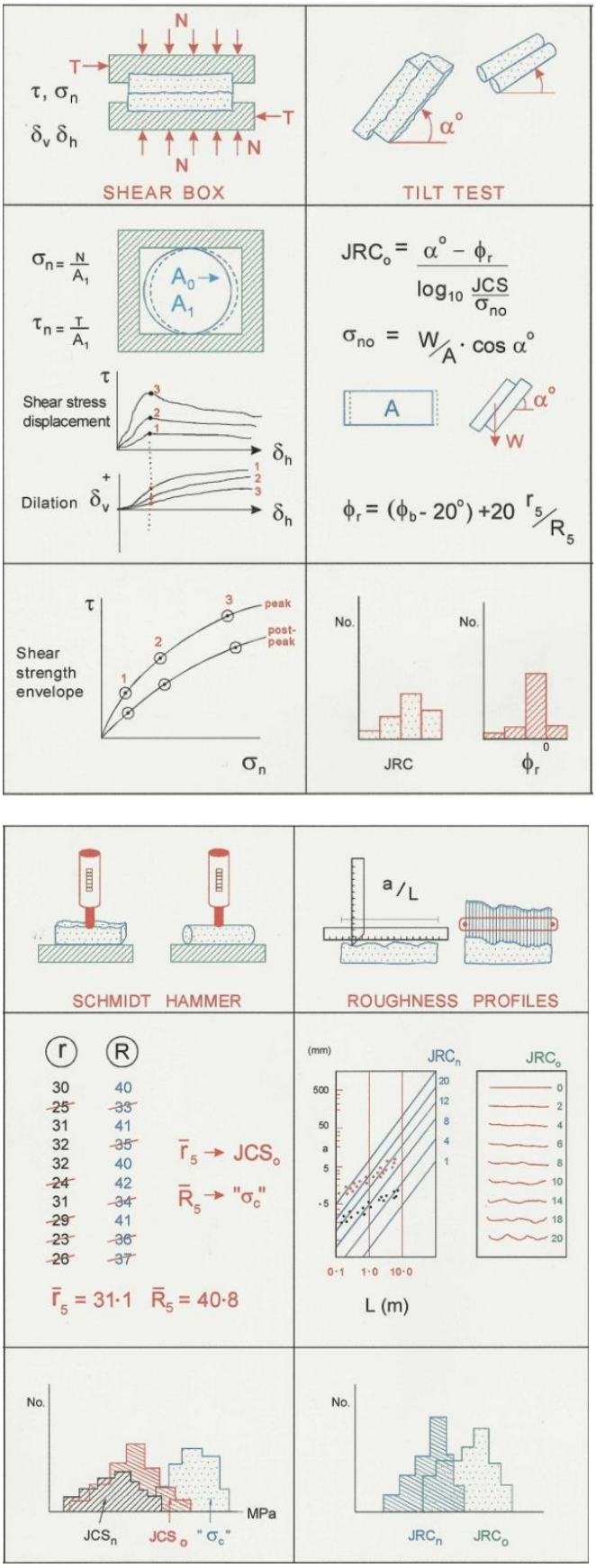

Figure 9. A synthesis of the simple index tests for obtaining input data for shear strength and coupled BB behaviour for tension fractures or natural rock joints, using tests on core or on samples sawn or drilled from outcrops. In the top- left column, direct shear tests are also illustrated, which can be used to verify the results from the empirically-derived index tests. This summary index-test figure is from Barton (1999).

Note that the Schmidt hammer should be used on clamped pieces of core to estimate the uniaxial compression strength UCS or σ_c. Rock density is needed as in the standard ISRM method. However, departing from ISRM, this test is done as follows: on dry pieces of core (rebound R, giving UCS: use *top 50% of results*). For the usually lower joint wall strength JCS, the rebound test is done on saturated samples (rebound r, use *top 50% of results*). These samples also need to be clamped (e.g. to a heavy metal base).Three methods of joint-wall or fracture-wall roughness (JRC) can be used: tilt tests to measure tilt angle α (Figure 8), or a/L (amplitude/length) measurement, (Figure 12), or roughness profile matching which is obviously more subjective.

A standard set of small-scale (length L_0 = 100 mm) roughness profiles was shown in Figure 7, and profiles of >1m (length L_n), with consequently reduced JRC_n values, are shown in Figure 10, from Bakhtar and Barton (1984).

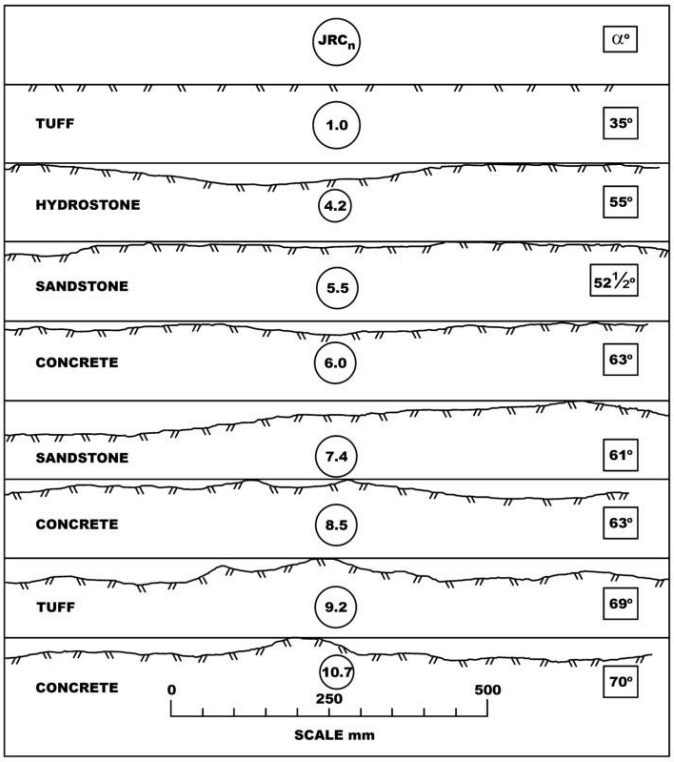

Figure 10. Tilt test JRC_n values. Bakhtar and Barton (1984).

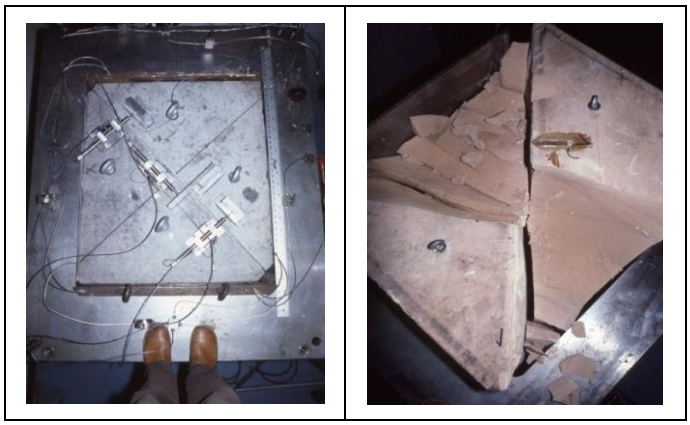

Figure 11. Larger-scale investigations of shear strength, using principal stress-driven tension fractures. Bakhtar and Barton (1984).

The 'a/L' method illustrated with typical scale-dependent data points in Figure 12 is based on the following empirical approximations. At 0.1m scale $JRC_0 \approx a/L \times 400$. At 1.0m scale, $JRC_n \approx a/L \times 450$, and at 10m scale (where there is inevitably little data) $JRC_n \approx a/L \times 500$. For example, with a/ L = 10mm/1000mm, the predicted JRC_n value, assuming typical 1m block sizes, would approximate 0.01 x 450 = 6. At 0.1 m scale, even 5mm roughness amplitude would suggest $JRC_0 \approx 20$.

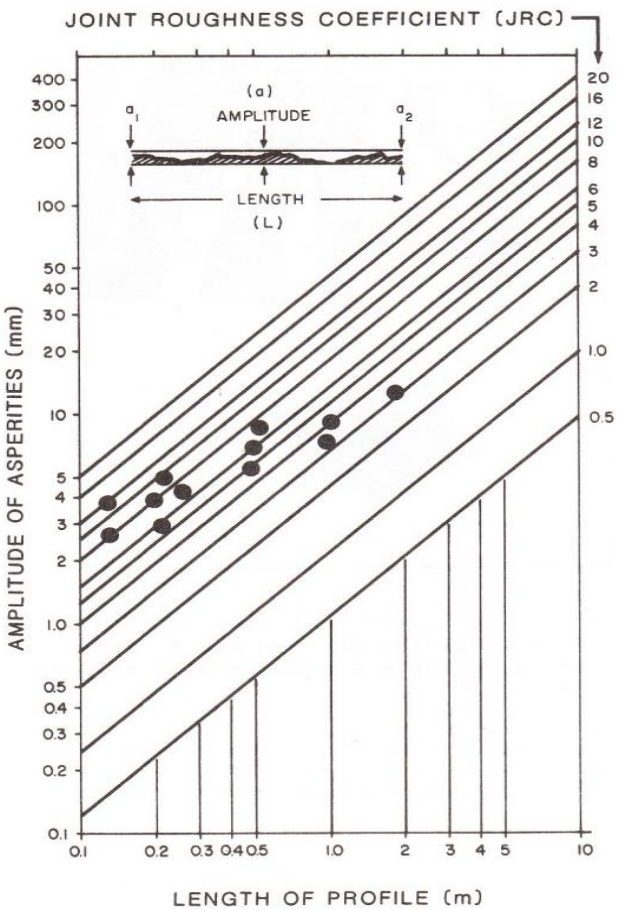

Figure 12. The 'a/L' amplitude over length method of estimating larger-scale joint roughness JRC_n, from Barton, 1982. Data points crossing the JRC lines indicate scale effects.

3.2 *Peak shear strength is only part of the behaviour*

It is natural that only the peak (or residual) shear strengths have been mentioned up to this point, although the DST (direct shear test) elements of behaviour have been illustrated in the left-hand column of Figure 9. In fact all the curves illustrated: $\tau - \sigma_n$ (peak strength envelopes), and the normal stress dependent $\tau - \delta_h$ (shear-displacement) and $\delta_v - \delta_h$ (dilation curves) can be simulated, and are in fact a part of the behaviour which is modelled in UDEC-BB, based on the BB (Barton-Bandis) sub-routine for non-linear joint behaviour. This is known to give different results to the commonly used UDEC-MC (Mohr-Coulomb-based linear simplifications).

Figure 13 illustrates the dimensionless model known as '$JRC_{mobilized}$' in which widely varying strength-displacement data acquired over a range of normal stress can be 'compressed' into a narrow band, using these dimensionless axes.

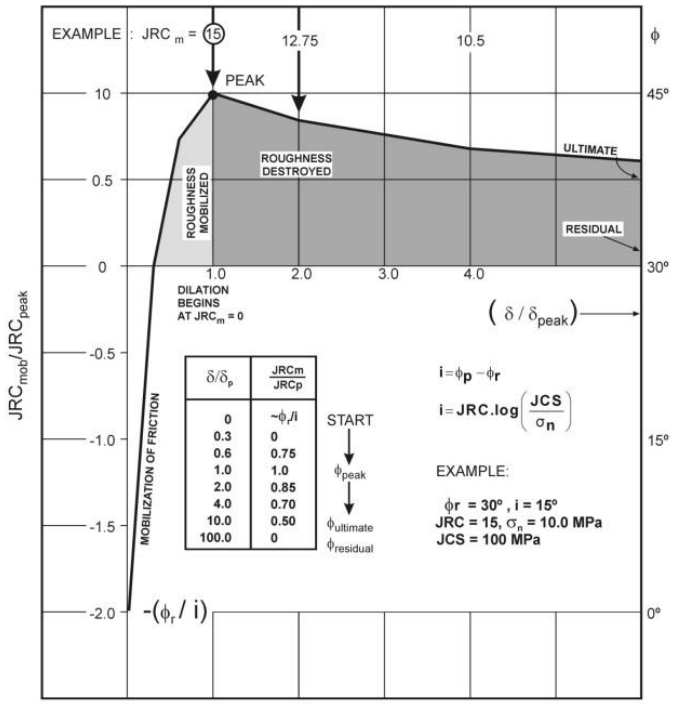

Figure 13. Peak shear strength is not reached until it is mobilized by pre-peak shearing, and *residual strength* is not reached until roughness has been destroyed by post peak shearing. (The latter needs tectonic events: the more likely is a higher 'ultimate' strength). Barton (1982).

Simulating (or predicting) the shear strength – shear displacement behaviour of rock joints at 0.1m, 1.0m and 2.0m scales is demonstrated in Figure 14. This scale refers to block size, as given by the spacing of cross-joints in a bench or open-pit stability assessment. A quite high (JRC_0 = 15) roughness was deliberately used in this hand-calculated demonstration, in order to show strong potential scale effects.

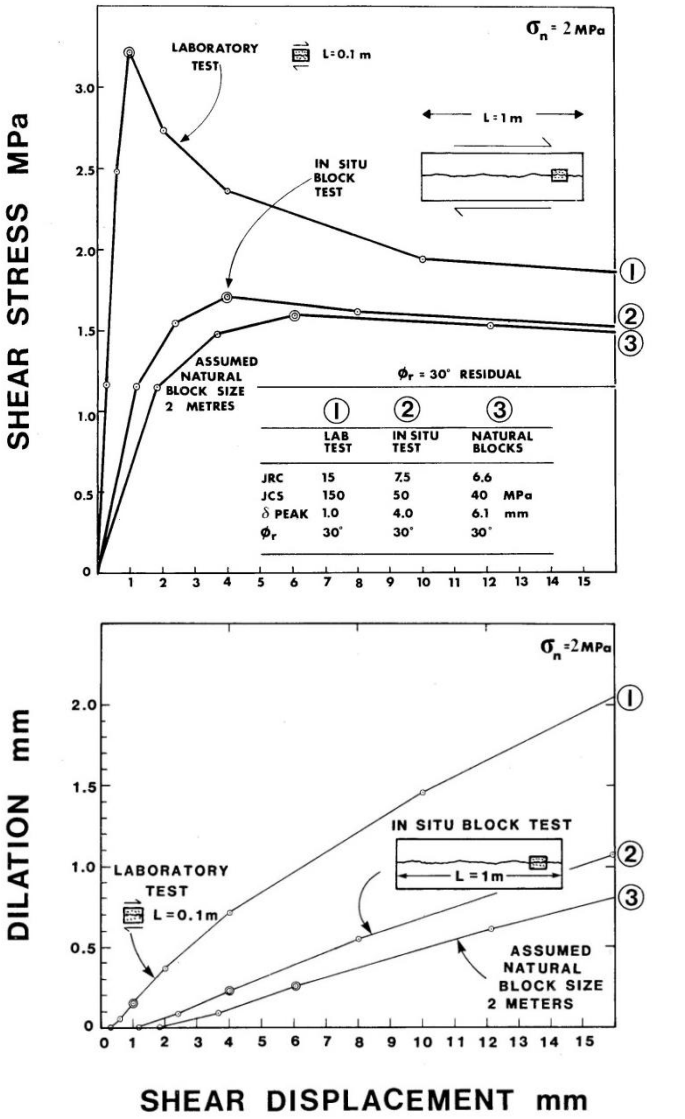

Figure 14. Shear stress-displacement curves for three different block sizes (0.1, 1.0 and 2.0m), and the corresponding dilation curves.The dilation modelling is described in Barton, 1982 and is part of UDEC-BB. All these curves were readily generated 'by hand'. This is is greatly in contrast to later H-B algebra.

The scaling of JRC_0 and JCS_0 shown in the inset to Figure 14, is made by following Bandis et al. (1981) empirical scaling laws. These are shown in Figure 15 with the accompanying equations.

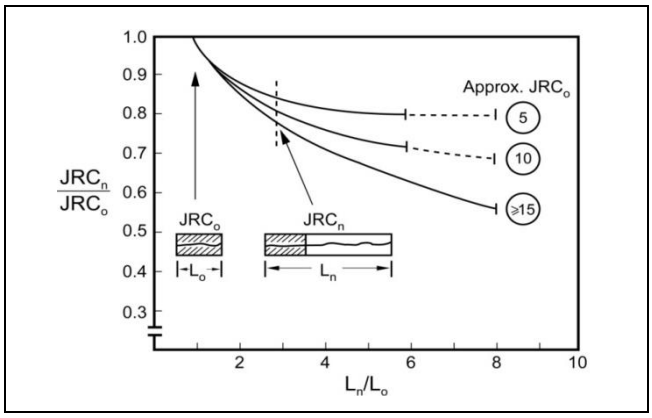

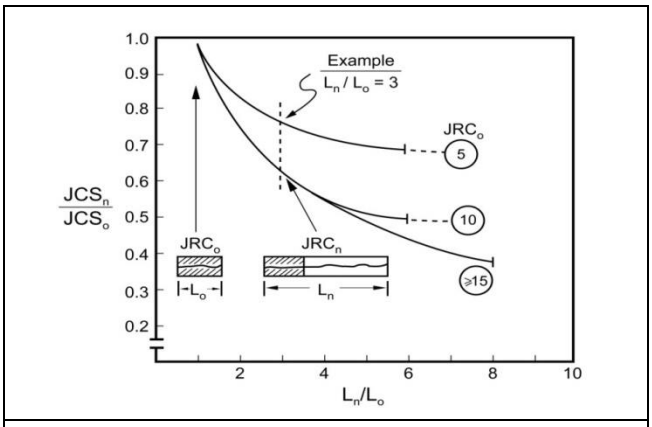

$$JRC_n \approx JRC_o \, [\, L_n/L_o \,]^{-0.02\, JRC_o}$$

$$JCS_n \approx JCS_o \, [\, L_n/L_o \,]^{-0.03\, JRC_o}$$

Figure 15. Empirical scaling rules for JRC (peak) and JCS. Note that scaling is needed whenever one performs direct shear tests, whether using linear Mohr-Coulomb or this non-linear Barton-Bandis strength criterion. The only exceptions would be planar joints, or if large enough *in situ* tests were performed, corresponding to natural block size. Bandis et al. (1981).

Before leaving the subject of shear strength for rock joints, it is important to emphasize the *absence of cohesion* when direct shear testing the vast majority of rock joints, even those which are extremely rough. Figure 16 shows the peak strength test results obtained from 130 individual rock joints sampled from seven different rock types, from Barton and Choubey, 1977. These were not replicas as was recently referred in remarkably out-of-touch literature.

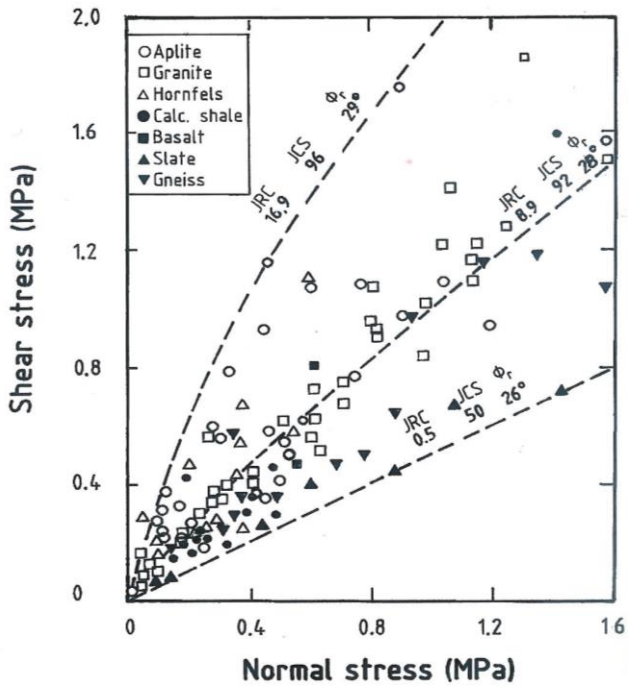

Figure 16. The peak strength of 130 rock joints, direct shear tested only once, following tilt-test characterization at ≈ 0.001 MPa. The ISRM suggested method, which includes multi-stage testing, creates artificial 'cohesion' because of clockwise rotation of strength envelopes. This practice should be avoided.

4 MODELLING OF ROCK MASSES

Figure 5 contained three (or four) conceptual components of shear strength of real rock masses: 1. the intact rock (i.e. intact 'bridges'), 2. the freshly developed fractures (formed at the instant that the 'bridges' have failed), 3. the shear strength of the surrounding and probably several sets of rock joints (with one set typically dominant in continuity), 4. eventual clay-filled discontinuities, including faults (See Figure 18 for guidance here). *Each of the above reach peak shear strength at different strains.* It is therefore that the adding of 'c' and σ_n tan'φ', (worst of all in a linear Mohr-Coulomb format), are two of the most erroneous things commonly performed in rock engineering. We need to degrade 'c' at small strain, and mobilize 'φ' at larger strain, strictly speaking with high JRC, JCS and φ_b for the newly formed fractures, and with lower JRC, JCS and φ_r for the joints, starting with the set with highest stress/strength ratio. The features with least shear-resistance will be the clay-filled discontinuities and faults. These are often involved in pit slope failure.

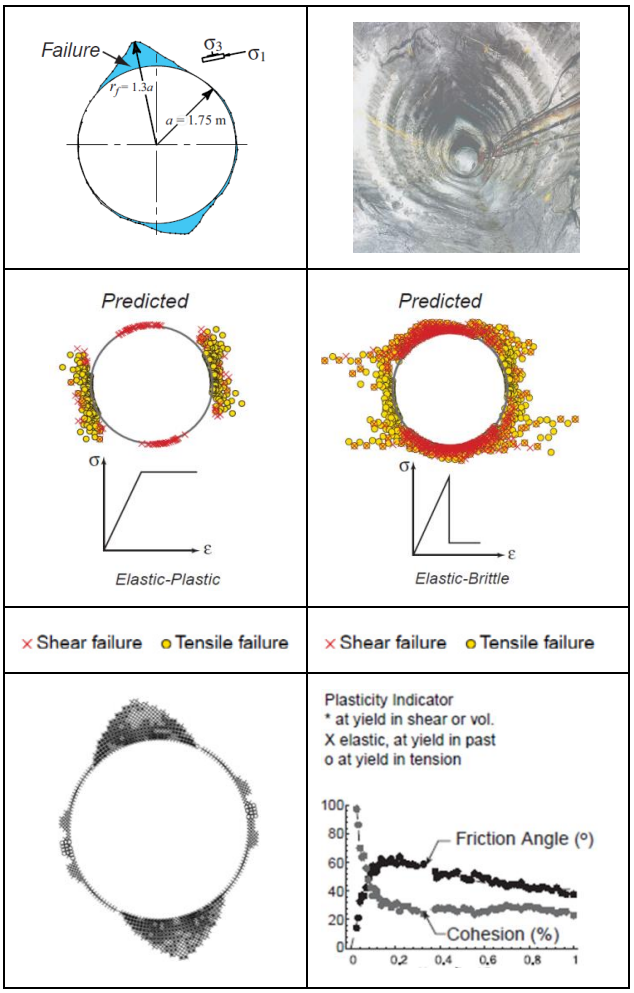

Figure 17. A demonstration of the challenge faced in the world of standard-methods rock mechanics modelling. The stress-induced failure (top) is unrealistically modelled using Mohr-Coulomb (and Hoek-Brown) strength criteria. However a 'c' *then* 'σ_n tan φ' (degrade/mobilize) approach gives a realistic plastic zone in FLAC. Hajiabdolmajid et al. (2000).

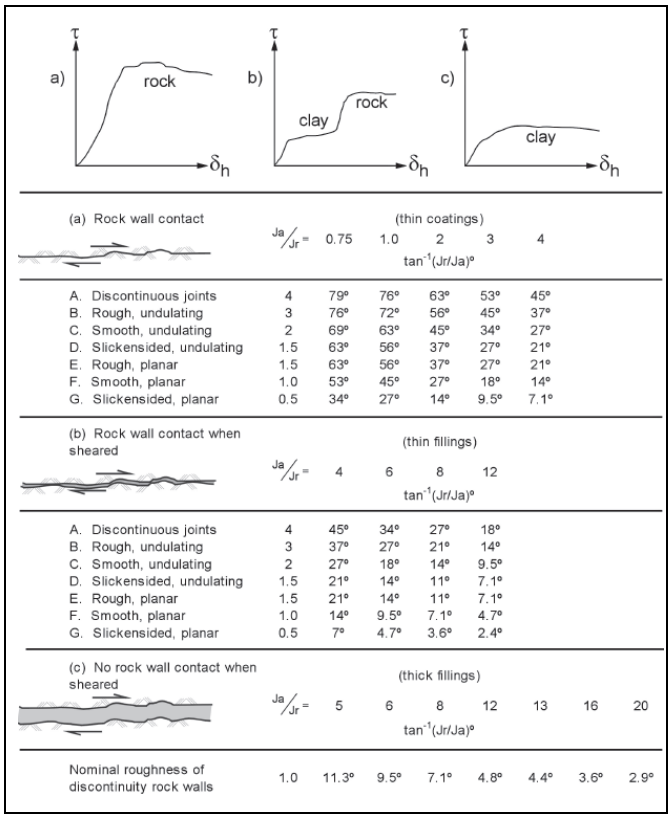

(a) Rock wall contact	Ja/Jr = 0.75	1.0	2	3	4
	tan⁻¹(Jr/Ja)° (thin coatings)				
A. Discontinuous joints	4	79°	76°	63°	53°	45°
B. Rough, undulating	3	76°	72°	56°	45°	37°
C. Smooth, undulating	2	69°	63°	45°	34°	27°
D. Slickensided, undulating	1.5	63°	56°	37°	27°	21°
E. Rough, planar	1.5	63°	56°	37°	27°	21°
F. Smooth, planar	1.0	53°	45°	27°	18°	14°
G. Slickensided, planar	0.5	34°	27°	14°	9.5°	7.1°

(b) Rock wall contact when sheared	Ja/Jr = 4	6	8	12
	tan⁻¹(Jr/Ja)° (thin fillings)			
A. Discontinuous joints	4	45°	34°	27°	18°
B. Rough, undulating	3	37°	27°	21°	14°
C. Smooth, undulating	2	27°	18°	14°	9.5°
D. Slickensided, undulating	1.5	21°	14°	11°	7.1°
E. Rough, planar	1.5	21°	14°	11°	7.1°
F. Smooth, planar	1.0	14°	9.5°	7.1°	4.7°
G. Slickensided, planar	0.5	7°	4.7°	3.6°	2.4°

(c) No rock wall contact when sheared	Ja/Jr = 5	6	8	12	13	16	20
	tan⁻¹(Jr/Ja)° (thick fillings)						
Nominal roughness of discontinuity rock walls	1.0	11.3°	9.5°	7.1°	4.8°	4.4°	3.6°	2.9°

Figure 18. Some guidance on the possible lowered friction angles for clay-filled discontinuities can be obtained from this Q-system based method. Note that the friction angles estimated from $\tan^{-1}$(Jr/Ja) resemble 'φ+ i', 'φ' and 'φ-i' due to dilation (top-left in tables), no dilation (central values in tables), or contraction (bottom-right in tables). In other words the case record basis for Jr and Ja ratings reflects the relative degree of stability or instability. Barton (2002) based on Barton et al. (1974).

The Canadian URL mine-by break-out (Figure 17) developed when excavating by line-drilling, in response to the obliquely acting anisotropic stresses, has provided a modelling challenge to the profession, because of the important demonstration of *unsuccessful modelling* by the commonly used 'standard methods' (Hajiabdolmajid et al., 2000). The fact that this same study was followed by more realistic *degradation of cohesion and mobilization of friction*, applied in FLAC, should have alerted the profession of rock mechanics more than a decade ago. (Note that these authors' 6/02/1999 FLAC modelling date was removed for clearer presentation).

4.1 *Hoek-Brown algebra or CC then FC*

It is remarkable that so many utilize the computer-generated H-B/GSI curves of the assumed 'shear strength' of rock masses (See Table 1). An extremely *non*-transparent sequence of 'nested' algebra lies behind this *a priori* method. It neither encourages much thought, nor much needed research into the actual *process-and-strain-dependent* shear behaviour of rock masses, which has been outlined above. There can be no set of equations in regular use in

rock engineering which come close to matching all this surprising algebra. It is too easy to demonstrate complete lack of 'transparency', e.g. to an additional joint set, or to a clay-filled discontinuity.

Table 1 Hoek-Brown/GSI based algebra for 'c' and 'φ'. This is what lies behind the admittedly impressive-looking 'shear strength' curves promoted by RocScience. One may wonder what happens if an extra joint set or clay-filling is added.

$c' = \dfrac{\sigma_{ci}\left[(1+2a)s+(1-a)m_b\sigma'_{3n}\right]\left(s+m_b\sigma'_{3n}\right)^{a-1}}{(1+u)(2+a)\sqrt{1+\left(6am_b\left(s+m_b\sigma'_{3n}\right)^{a-1}\right)\Big/\left((1+a)(2+a)\right)}}$
$\phi' = a\sin\left[\dfrac{6am_b\left(s+m_b\sigma'_{3n}\right)^{a-1}}{2(1+a)(2+a)+6am_b\left(s+m_b\sigma'_{3n}\right)^{a-1}}\right]$
$m_b = m_i \,.\, e^{(GSI-100)/(24-14D)}$
$s = e^{(GSI-100)/(9-3D)}$
$a = ½ + 1/6\,(e^{-GSI/15} - e^{-20/3})$

Following the simple development of the Q to Q_c normalization ($Qc = Q \times \sigma_c/100$) to obtain better fit to seismic velocity and deformation modulus, it was discovered (Barton, 1995, 2002) that Q_c seemed to be composed of 'c' x tan 'φ'. There is no misprint: the multiplication is correct. This means that Q_c = CC x FC (where Q_c = RQD/Jn x Jr/Ja x Jw/SRF x $\sigma_c/100$. CC and FC are therefore as follows:

CC = (RQD/Jn) x σ_c/(100.SRF) (1)
(the component of a rock mass requiring shotcrete for tunnel support, if the value of CC is too low)
FC = (Jr/Ja) x Jw (2)
(the component of a rock mass requiring bolting for tunnel reinforcement, if the value of FC is too low)

The ultra-simple and *claimed* CC and FC links to Q-system case-record needs for *shotcrete and bolting* will obviously also seem far-fetched, perhaps until examples of CC and FC are presented, in relation to realistic rock mass conditions. Table 2 shows some examples, and includes links to P-wave velocities and deformation moduli (Barton, 2002).

Table 2. Realistic Q-parameterization of successively more jointed, clay-bearing and generally weaker rock masses, and the simply estimated strength components CC (resembling cohesion in MPa) and $\tan^{-1}$(FC)° resembling friction angle φ.

RQD	Jn	Jr	Ja	Jw	SRF	Q	σ_c	Q_c	FC°	CC	V_p	E_m
100	2	2	1	1	1	100	100	100	63	50	5.5	46
90	9	1	1	1	1	10	100	10	45	10	4.5	22
60	12	1.5	2	0.66	1	2.5	50	1.25	26	2.5	3.6	11
30	15	1	4	0.66	2.5	0.1	33	0.04	9	0.3	2.1	3.5

Note: σ_c (MPa), CC (resembling MPa), V_P (km/s), E_m (GPa).

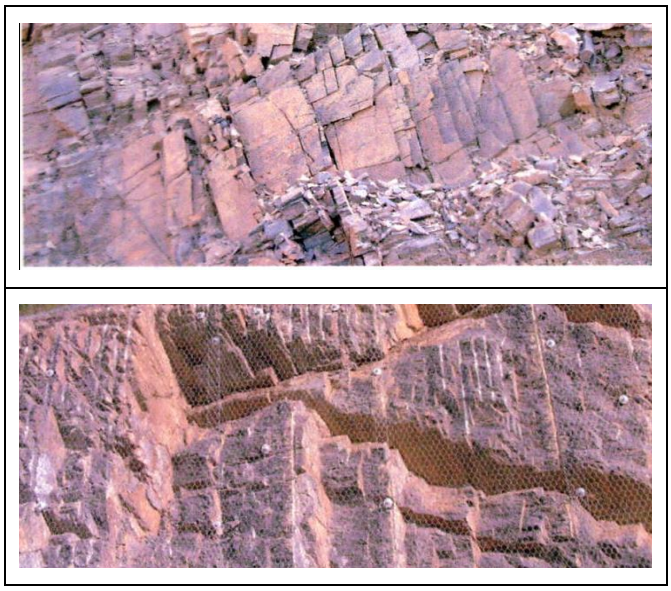

Figure 19. Examples of two contrasting rock masses which demonstrate a clear need for S(fr) and B respectively, due to insufficient CC and FC or low 'c' and low 'φ'. Of course B+S(fr) could be applied in both cases, but the local solutions were respectively S(fr) alone, B alone, (but with a light mesh).

The preferred rock support and reinforcement required and used in Figure 19 are quite clear, and indeed in the original Barton et al. (1974) Q-system, there were *conditional factors* concerning relative block-size (RQD/Jn) and relative frictional strength (Jr/Ja), specifically for differentiating a recommended/preferred: *more shotcrete*, or more *rock bolts*.

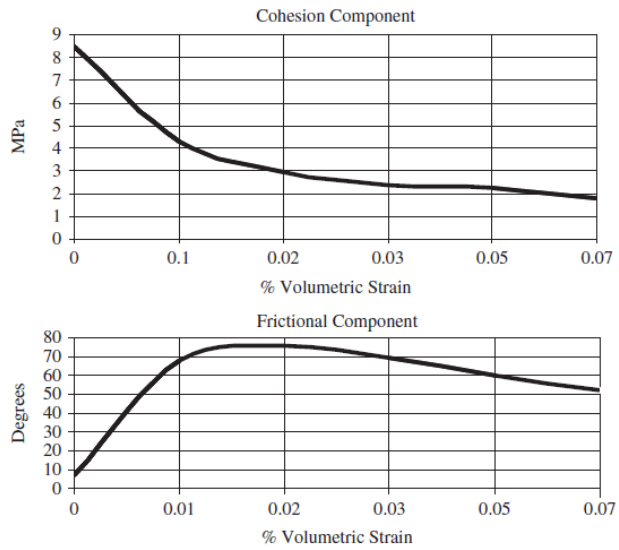

Figure 20. The degradation of 'c' (= CC) and the mobilization of 'φ' (= FC) used by Pandey in FLAC3D modelling.

The 'jointed continuum' thinking behind CC and FC is that these simple, very transparent parameters can be derived from Q-parameter mine statistics. This was the approach used in Barton and Pandey (2011), who reported FLAC3D modelling of multiple stopes in two Indian mines. (See Figure 21 example). The scale of the problem, as so often in min-

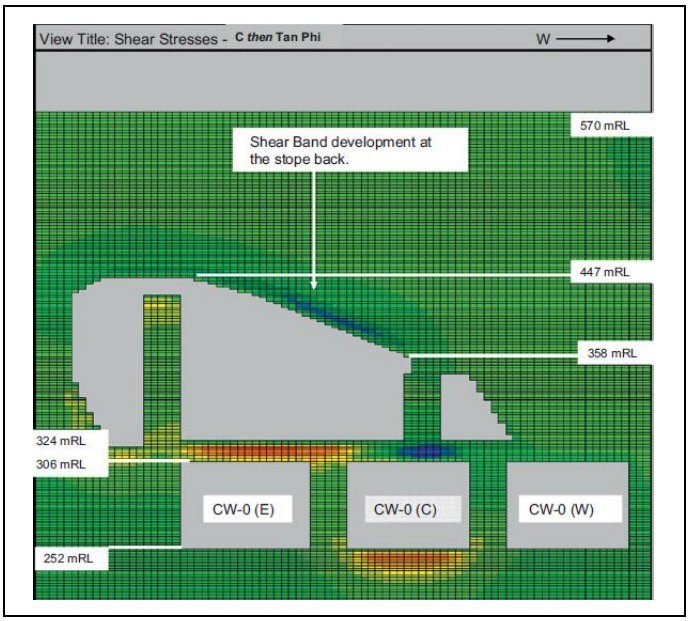

Figure 21. FLAC3D model (central region) using 'c then tan φ' (degraded cohesion CC) and mobilized friction FC). Barton and Pandey (2011). There are encouraging signs that others in the profession are testing this approach, and obtaining better matches with observed behaviour. See for instance Edelbro (2009), who utilized degradation/mobilization in Phase 2.

ing, precluded the initial performance of discontinuum analyses, with for instance UDEC or 3DEC, so the parameters CC and FC were assumed to be representative of a *pseudo-continuum* shear strength. An important departure from convention was the *degradation of CC and the mobilization of FC* (See Figure 20), following the suggestion in Hajiabdolmajid et al. (2000), as reproduced earlier in Figure 17. Reality was checked using the deformations registered with pre-installed MPBX and using the empirical displacement equations 4 and 5, with the mine-logged Q-values. According to mining colleague Pandey, who has rock mechanics responsibilities in eight Indian mines, the result of the 'c *then* tan φ' modelling, compared to the conventional 'c *plus* tan φ' modelling (with either Mohr-Coulomb or Hoek-Brown shear strength criteria), was greater realism and better matching to measured and empirically derived deformations (equations 4 and 5). The *realism* included the shear band development within the stope back: something that did not apparently occur with the conventional modelling.

4.2 *Deformation estimation using Q*

In Barton et al. (1994) the results of MPBX monitoring of the 62m span Gjøvik Olympic cavern were added to earlier data from 1980, using the plotting format *Q/SPAN versus deformation*, both on log-scales. The results are seen at the top of Figure 22. (Note 'increasing SRF' area). Some years later, Shen and Guo (priv. comm.) sent the second figure (Figure 22b) with hundreds of data points from tunnels

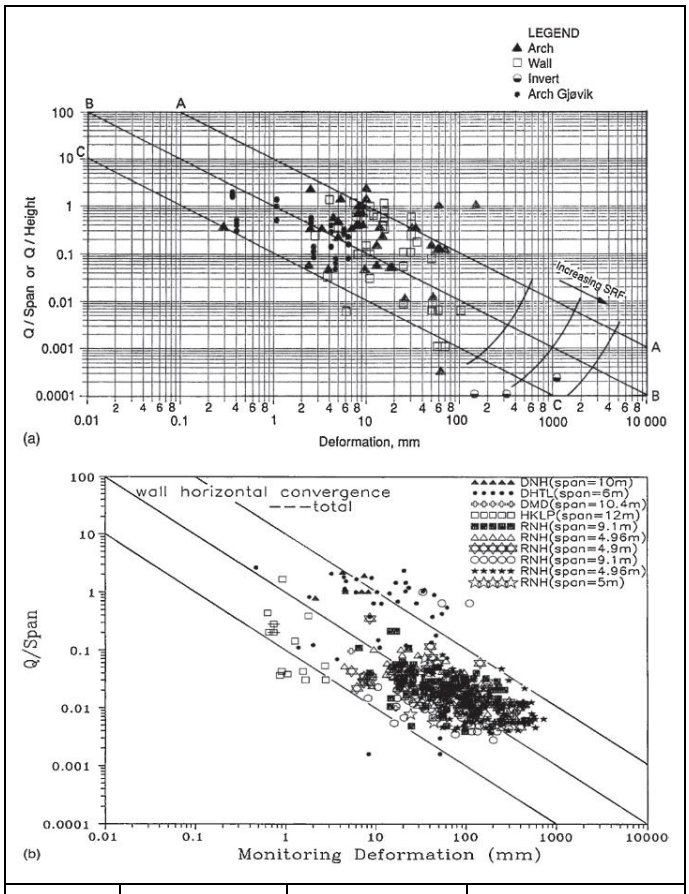

$\Delta = \frac{SPAN}{Q}$	$\Delta_v = \frac{SPAN}{100Q}\sqrt{\frac{\sigma_v}{\sigma_c}}$	$\Delta_h = \frac{HEIGHT}{100Q}\sqrt{\frac{\sigma_h}{\sigma_c}}$	$k_o = \left(\frac{SPAN}{HEIGHT}\right)^2\left(\frac{\Delta_h}{\Delta_v}\right)^2$

Figure 22. Q/span versus deformation data from Barton et al. (1994) with a large body of additional Taiwan tunnels data from Guo and Shen (priv. comm. due to Chinese language). Empirically-based improvements, to reduce the scatter, were given in Barton (2002). See equations 3, 4 and 5.

in Taiwan, and plotted in the same log-log format. It now became clear that the central-trend line was of interest. This proved to be simplicity itself:

$$\Delta = \frac{SPAN}{Q} \qquad (3)$$

where Δ is in mm, and SPAN is in meters. The ability to check *numerical modelling results*, using such empirical data, has been found useful, and on occasion modelling results have been found to be quite unrealistic (e.g. 10 x too high in case of exaggerated joint continuity being assumed in UDEC-MC and -BB models). The lack of reality may be seen both in relation to subsequent measurements when caverns are constructed, and in relation to the empirically-based predictions, using these two equations.

$$\Delta v \approx SPAN\,(\sigma_v/\sigma_c)^{0.5}\,/100\,Q \qquad (4)$$

$$\Delta_h \approx HEIGHT\,(\sigma_h/\sigma_c)^{0.5}\,/100\,Q \qquad (5)$$

where Δv, Δ_h , SPAN and HEIGHT are in *mm.*

Once again we see equations which are simple enough to remember, and transparent to alterations in input assumptions. As a simple demonstration: equation 3 suggests $\Delta = 62/10 = 6.2$ mm for the case of the 30 to 50 m deep Gjøvik cavern, where the most frequent Q = 10 (range 2 to 30). Both the MPBX measurements, and UDEC-BB modelling (Figure 23) showed Δ_v of about 7 mm. Equation 4, with prospects of greater accuracy, would suggest the following: Δ_v (mm) $\approx 62{,}000 \times (1/90)^{0.5}/100 \times 10 \approx 6.5$ mm.

4.3 *Depth dependent deformation modulus*

The FLAC3D stope modelling described by Barton and Pandey (2011) was performed using a surprisingly unusual but definitely needed *depth-dependent* deformation modulus, in addition to the *degradation* of CC immediately followed by *mobilization* of FC. It is indeed surprising that this depth-dependence does not seem to be practiced by those using GSI, perhaps because of the 'stress-free' deformation modulus formula shown in Table 3, since RMR and therefore GSI are apparently without a stress term.

The need for a modulus increase with depth was discussed and utilized by Barton et al. (1994) in UDEC-BB modelling, as seen in Figure 23. It is the subject of extensive review, together with a lot of data on V_P, in Barton (2006). Note that E_m at *nominal 25 m depth* is estimated from the central diagonal (heavy) line in Figure 25.

$$E_m \approx 10\, Q_c^{1/3} \quad \text{(units of GPa, see Fig. 25)} \qquad (5)$$

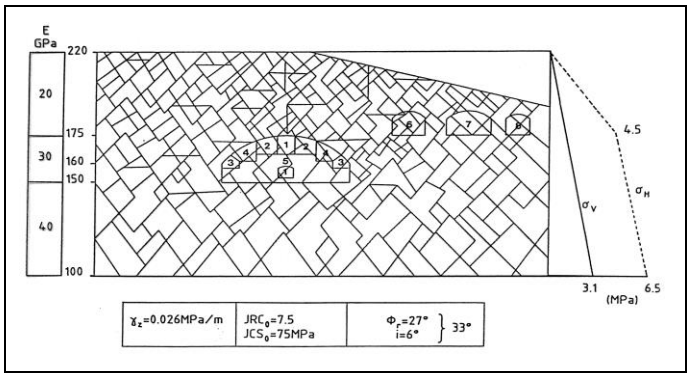

Figure 23. Gjøvik cavern input data assumptions for UDEC-BB modelling. Depth-dependent moduli are required for realistic numerical modelling, something that seems to have been neglected in some of our profession. Barton et al. (1994).

The 'phenomenon' (but it is surely obvious) of increased V_P and E_{mass} with depth was experienced in cross-hole seismic tomography at the Gjøvik 62m span cavern site (Barton et al. 1994) in jointed granites, and also in jointed chalk by Hudson and New, 1980. (See details in Barton, 2007). In both cases there was *no improvement of quality* with depth, yet

Table 3. A comprehensive comparison: GSI-based and Hoek-Brown (and Diederich) estimations for modulus (with infinitely flexible D = 0 to 1 for disturbance), rock mass strength, 'φ' and 'c', compared with the simplicity and transparency of Q-based formulations. The advantage of Q is its six orders of magnitude. RMR and GSI are at a disadvantage here, therefore the complex and remarkably opaque algebra. The user is lost.

$$E_m\,(GPa) = \left(1-\tfrac{D}{2}\right)\sqrt{\tfrac{\sigma_{ci}}{100}} \times 10^{(GSI-10)/40}$$

$$\sigma'_{cm} = \sigma_{ci} \times \frac{(m_b+4s-a(m_b-8s))\,(m_b/4+s)^{a-1}}{2(1+a)\,(2+a)}$$

$$\varphi' = a\sin\left[\frac{6am_b(s+m_b\sigma'_{3n})^{a-1}}{2(1+a)(2+a)+6am_b\,(s+m_b\sigma'_{3n})^{a-1}}\right]$$

$$c' = \frac{\sigma_{ci}[(1+2a)s+(1-a)m_b\sigma'_{3n}]\,(s+m_b\sigma'_{3n})^{a-1}}{(1+u)\,(2+a)\sqrt{1+(6am_b(s+m_b\sigma'_{3n})^{a-1})/((1+a)\,(2+a))}}$$

where

$$\sigma_{3n} = \sigma'_{3\,max}/\sigma_{ci} \quad (+\mathrm{GSI}+a+s+m_b \text{ relations})$$

$$E_m \approx 10 \times Q_c^{1/3}$$

$$\sigma_{cm} \approx 5\gamma\, Q_c^{1/3}$$

$$\varphi \approx \tan^{-1}\left(\frac{J_r}{J_a} \times \frac{J_w}{1}\right)$$

$$c \approx \left(\frac{RQD}{J_n} \times \frac{1}{SRF} \times \frac{\sigma_c}{100}\right)$$

a significant increase in seismic P-wave velocity, as illustrated in Figure 24. A large body of deep seismic cross-hole tomography and corresponding Q-logging of all the core, to e.g. 1,100 m depth has

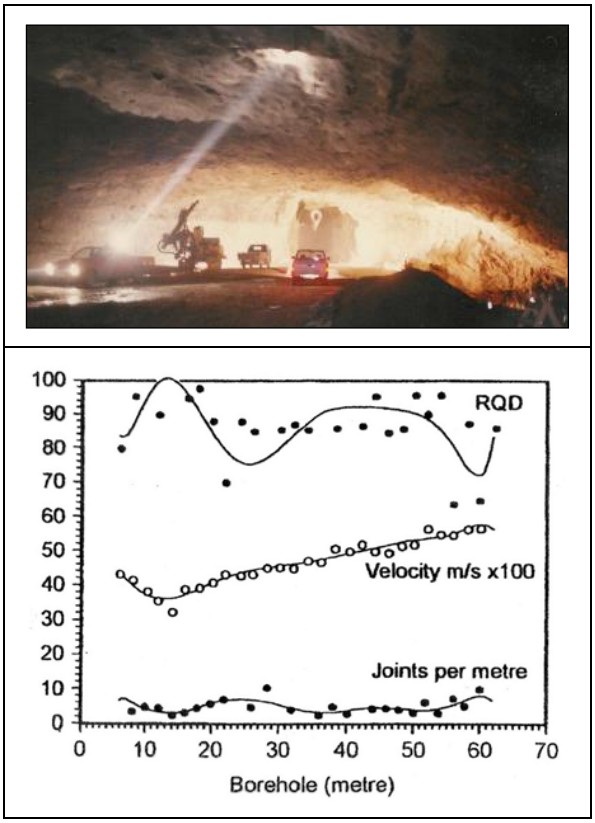

Figure 24. The top-heading of the 62m span Gjøvik cavern. Cross-hole seismic tomography and core logging demonstrated increased V_P (+ 2 km/s) with only 50m depth increase, yet no improvement of RQD or joints/m (or Q) i.e. a stress and joint closure effect, also affecting a deformation modulus increase.

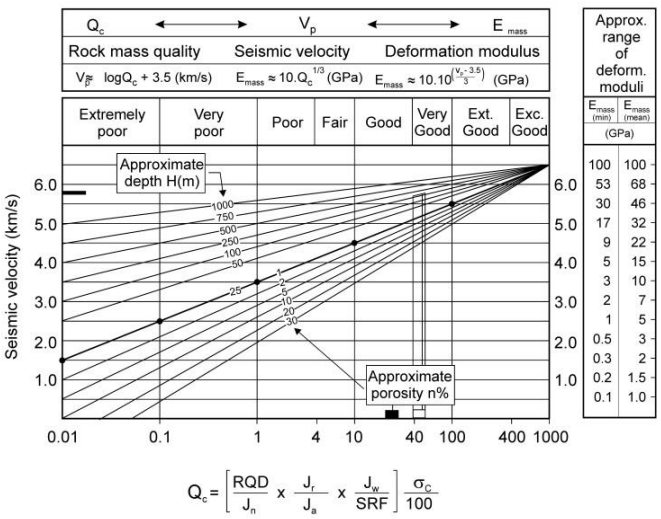

Figure 25. Integration of Q_c, V_P and $E_{mass.}$ Based on Barton (1995, 2002, 2006). Note that the empirical equations refer to the central 25m depth line. Example from 450m depth in Äspö.

been included in this documentation of depth-V_P trends. Figure 25, modified from Barton (1995) and (2002), shows E_{mass} (static deformation modulus), with the addition of the multiplier $Q_c = Q \times \sigma_c/100$ in order to improve fit to seismic and deformation data. The vertical bar drawn in Figure 25 is designed to lead the reader from observed Q-values of mostly 20-25, based on 800 m of core logging by former NGI colleague Løset. This was converted to Q_c = 40 to 50, due to UCS (σ_c) = 200 MPa (from $Q_c = Q \times \sigma_c/100$). The vertical bar is then followed upwards to 450m depth, where a predicted V_P of 5.8-5.9 km/s is shown. This is consistent with both the results of Calin Cosma's cross-hole seismic tomography performed for SKB around a little damaged trial drill-and-blast excavation (the ZEDEZ project), and with the deformation moduli of 65-70 GPa needed for UDEC modelling to match measured deformations.

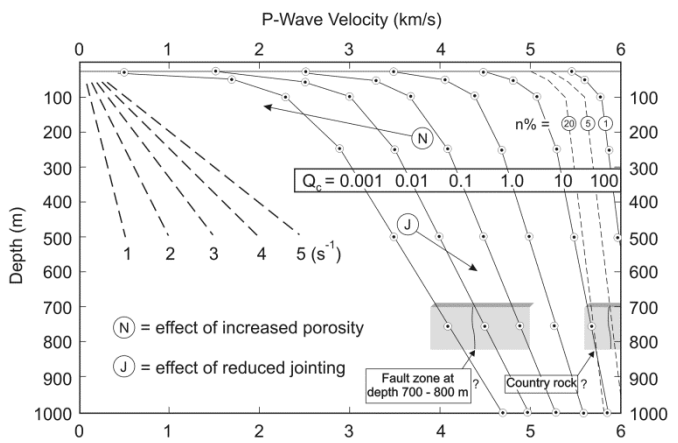

Figure 26. The depth dependence of V_P (which is integrated with E_{mass}) means that *Q_c isolines* can be drawn as a function of V_P-depth (as here) and as a function of E_{mass}-depth. In other words for unchanged Q or Q_c, both modulus and V_P increase with depth, due to (obvious) joint closure and normal stiffness K_n effects. Note the compression effect on deep fault zones.

Returning to near-surface equation 5, a deformation modulus at *nominal 25m depth* of only 34-37 GPa is predicted with Q_c = 40-50 (refer to solid central diagonal line in Figure 25). Likewise, V_P at *nominal 25m depth* would be expected to be only 5.1-5.2 km/s. However, at 450 m depth (with the addition of approximately 10-12 MPa of confining pressure: estimated from $\gamma H/100$), and using the increased measured V_P of 5.8-5.9 km/s, one would then be able to estimate an (also) elevated deformation modulus of approx. 75 GPa. This has been estimated from a more generally applicable equation 6, from Barton (2007a). It is written in a format independent of Q or Q_c, and suggests significantly higher deformation moduli when V_P measurements are also higher due to stress (joint closure) effects.

$$E_{mass} \approx 10^{(Vp - 2.5 + \log \sigma_c)/3} \qquad (6)$$

Table 4. Some examples of depth-dependent (because V_P dependent) deformation moduli E_{mass} using equation 6.

V_P (km/s)	2.5	3.5	4.5	5.5	6.5
σ_c (MPa)	10	100	100	150	150
E_{mass} (GPa)	2.2	10.0	21.5	53.1	114

5 SHEAR STRENGTH OF ROCKFILL

Since we have a (non-linear) constitutive model for rock joints, and since the shear strength of rock fill is almost indistinguishable from that of rock joints, this section can be brief and mostly visual for rapid communication. In Figure 5 the similarity of the two (due to 'points of contact' in common) was emphasized. Results of large-scale triaxial tests from which peak τ-σ_n data are derived, are discussed in Barton and Kjærnsli, (1981) and Barton (2008).

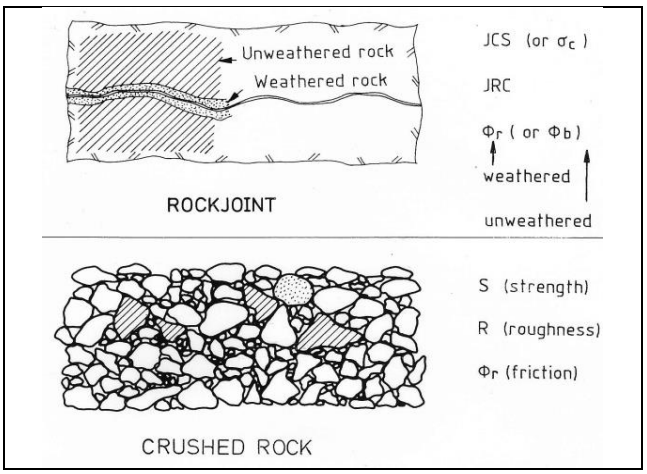

Figure 27. The equivalence of rock joints and crushed rock is due to 'points in contact', based on the supposition that at peak shear strength, the points in contact (asperities and stones) have reached their compressive strength limit (JCS or S). Various aspects of the shear strength of rock fill are illustrated in Figures 28 to 32. This includes consideration of interface strength.

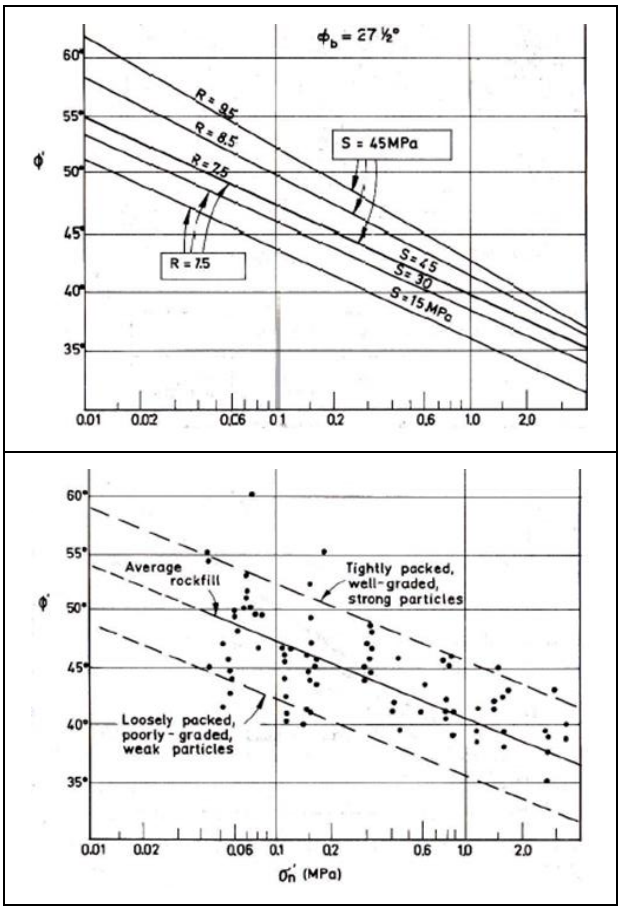

Figure 28. The well known collection of rockfill strength data from Leps (1970), and equivalent strength curves (log-linear lines) using R and S.

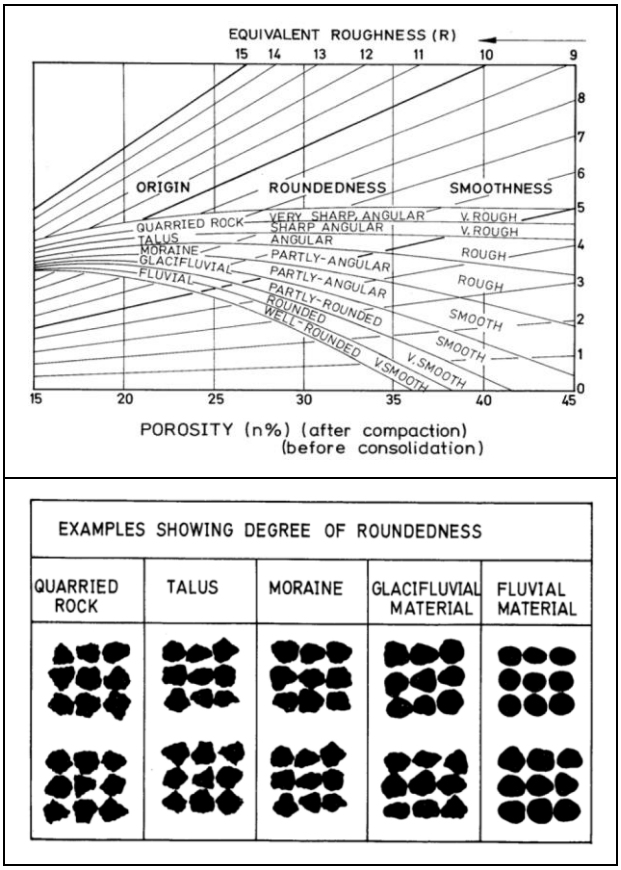

Figure 29. A simple way to estimate R based on the degree of smoothness, roundness, and origin, plus the porosity of the rock dump (or compacted rockfill dam).

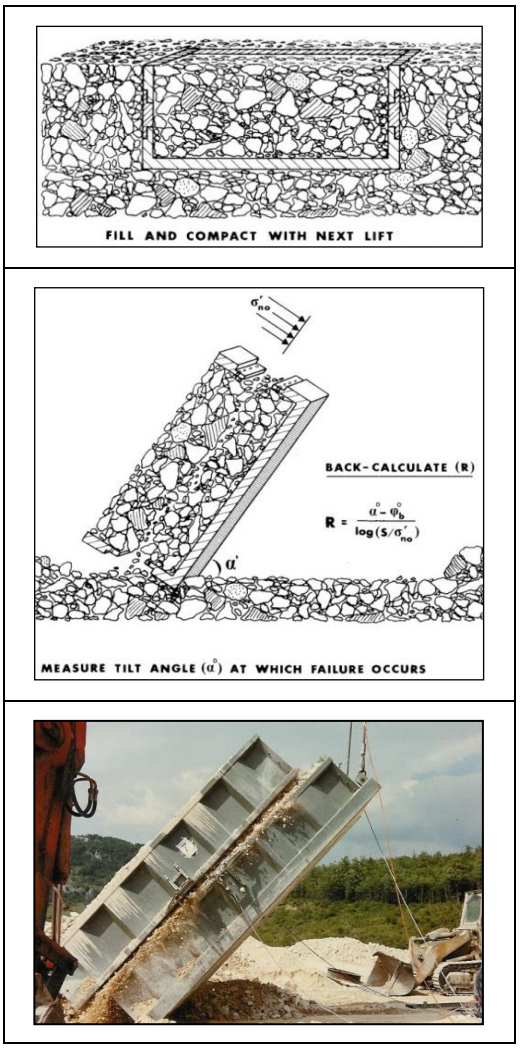

Figure 30. Large-scale tilt tests with actual 1:1 gradings of particle sizes have been performed. In the photograph, a tilt-box of 5 x 2 x 2 m dimensions is shown, which, following the principle of Barton and Kjærnsli, 1981, was excavated from a compacted lift of the dam in question, and then tilt tested in order to back-calculate R. Note that S is a d_{50} stone size estimate of UCS, based on strength scaling in Barton and Kjærnsli (1981).

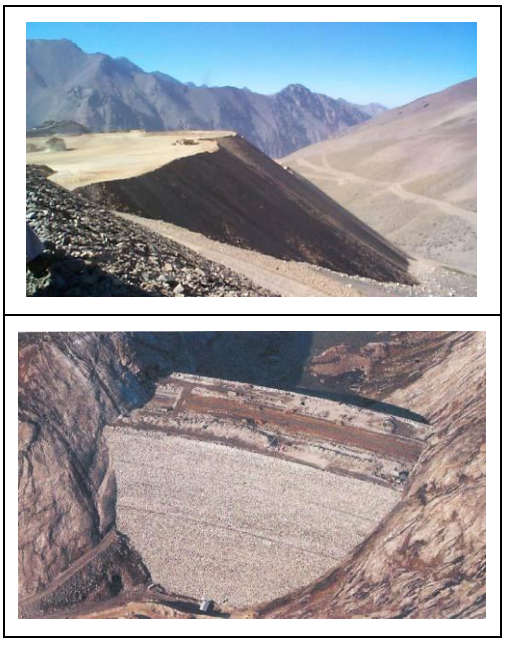

Figure 31. Rock dumps or dams: interface shear strength may sometimes be an issue. Top photo: Linero, bottom photo: NGI.

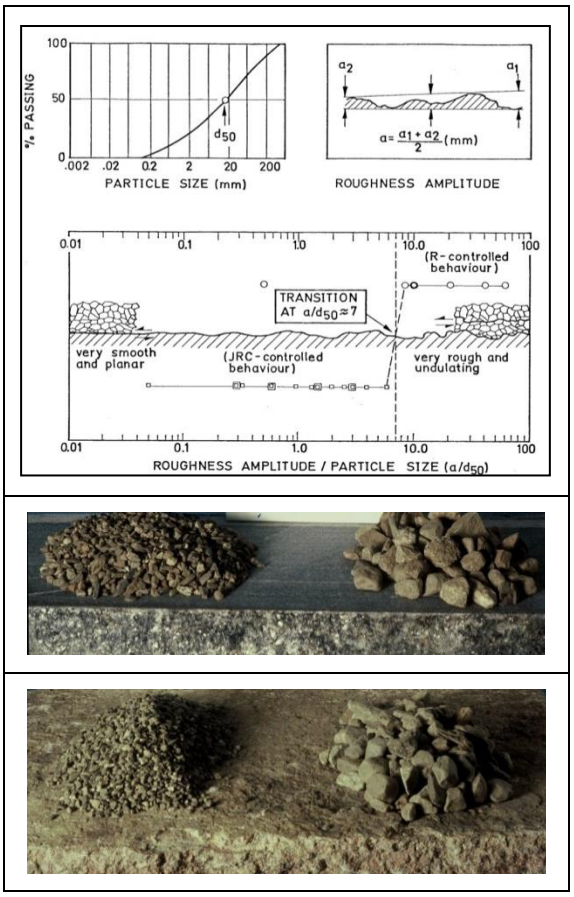

Figure 32. Using a similar 'a/L' method as used to estimate JRC for a rock joint (Figure 12), JRC-controlled *interface sliding*, and R-controlled (*inside-the-rockfill*) shearing can be distinguished, using a / d_{50} > 7. Only one of the four situations photographed have sufficient interlock to prevent interface sliding (Answer: bottom left). One can test this with tilt tests.

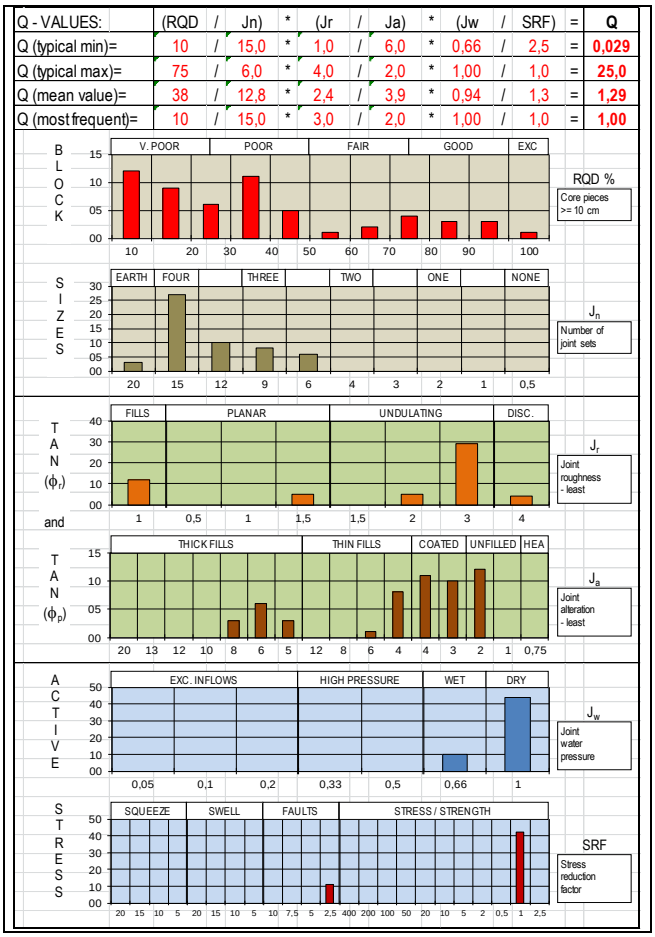

Figure 33. The Q-parameter statistics should be collected and presented when logging Q, because a given Q-value is not 'unique' and the structure of the parameter ratings which lie behind e.g. Q_{mean} often contain invaluable information, obviously superior to Q (or RQD) alone.

6 Q-PARAMETER STATISTICS FOR ZONING

The writer has noted the frequent use of the Q-system in various roles in mining. These include the use of Q' (or N) for stope behaviour prediction, Q-system support and reinforcement guidelines for permanent mine roadways, and Q-value based 'geotechnical zoning' for future or present mining resources. A point to remember when logging Q-parameters is that, although they form a helpful number with which to communicate an impression of rock quality (or lack of quality), there is important information 'coded' in the individual parameters. In this context it is useful to collect, and present, the statistical spread of data, as in the form of Q-parameter histograms, as illustrated in Figure 33. Nevertheless it is always important to be aware that the six Q-parameters are only an abbreviated description of the rock mass, as can be seen in Figure 34. The 'relative block size' (RQD/Jn) is just part of the *rock mass structure*, and the *shear strength* (Jr/Ja – which is actually like a friction coefficient), is a relatively simple part of the joint characterization.

I	ROCK MASS STRUCTURE			
1	RQD	Deere et al., 1967)	block size	Q
2	J_n	= joint set number		Q
3	F	= joint frequency (per metre)		
4	J_v	= volumetric joint count (Palmström, 1982)		
5	S	= joint spacing (in metres)		
6	L	= joint length (in metres)		
7	w	= weathering grade (ISRM, 1978)		
8	α/ß	= dip/dip direction of joints (Schmidt diagram)		
II	JOINT CHARACTER			
9	J_r	= joint roughness number	shear strength	Q
10	J_a	= joint alteration number		Q
11	JRC	= joint roughness coefficient		
12	a/L	= roughness amplitude of asperities per unit length (mm/m)		
13	JCS	= joint wall compressive strength		
14	ϕ_r	= residual friction angle		
15	r,R	= Schmidt rebound values for joint and rock surfaces		
III	WATER, STRESS, STRENGTH			
16	J_w	= joint water reduction factor	active stress	Q
17	SRF	= stress reduction factor		Q
18	K	= rock mass permeability (m/s)		
19	σ_c	= compressive strength		
20	σ_1	= major principal stress		

Figure 34. The pairs of Q-parameters, and their role.

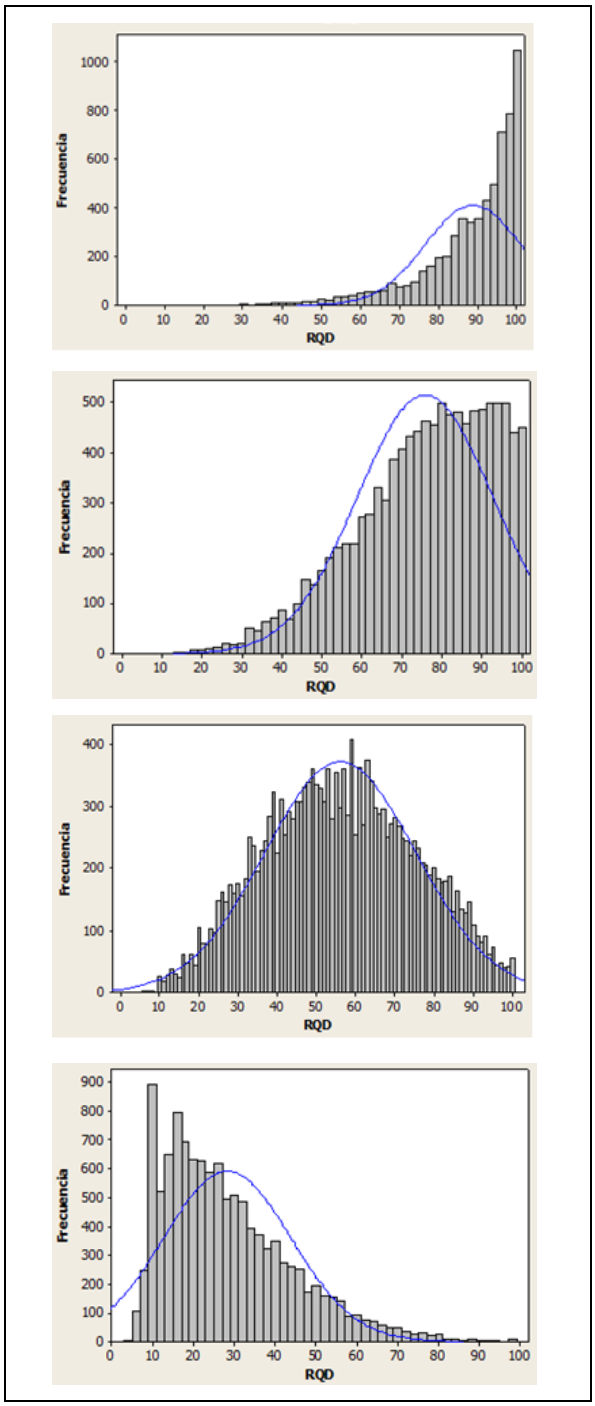

Figure 35. Q-classes 2, 3, 4 and 5, with respective Q-ranges as follows: 40-10, 10-4, 4-1, 1-0.1, and respective numbers of observations of RQD numbering approximately 6,000, 10,500, 18,000, 10,400, demonstrates the central role played by RQD in commonly experienced rock mass conditions.

On the subject of geotechnical zoning of future or existing mining resources, the use of Q-parameter statistics – in graphic format – can be extremely useful for better evaluation of Q-value based support of mine roadways (see next section). On occasion, the writer has been confronted with 'kilometers' of EXCEL tables, showing Q-logging and RMR-logging results, perhaps from tens or hundreds of kilometers of logged core. However well arranged in 'tabular form', it is in graphic format as in Figure 35, that the 'outsider' can more easily check for the reasonableness of the sometimes very extensive Q-logging already performed. Figure 35 illustrates, with just the use of RQD, how re-arranged (i.e. graphed) EXCEL data can be more easily assimilated when in visually varying format. Similar 'crossing-the-graph' histograms of other Q-parameters are seen when comparing Q-value classes like 1-4, 4-10. 10-40. The sometime critique of RQD needs to be silenced, especially since RQD *generally* stretches far beyond the short-sighted theoretical '<10 cm, > 10 cm' arguement in practice, due to the three dimensional nature of jointing and due to anisotropy. To obtain consistent RQD = 100 recordings a quite massive rock mass is required, one that for instance slows TBM progress due to large block sizes. RQD is a particularly sensitive parameter for rock engineering problem areas, and has survived 50 years of use because of this. RQD is particularly sensitive to the general rock class – and it partly 'sets the scene' for the overall Q-value – despite obviously missing some important details if used as a stand-alone parameter.

Figure 36. Photos of core with the following Jr values: Jr = 1.0 or 1.5, Jr = 1.5, Jr = 1.5, Jr = 1.5, Jr = 2, Jr = 2.5, Jr = 3.5.

Figure 36 was assembled recently in order to provide guidance for those logging core (or core photos), to obtain consistent joint roughness numbers Jr.

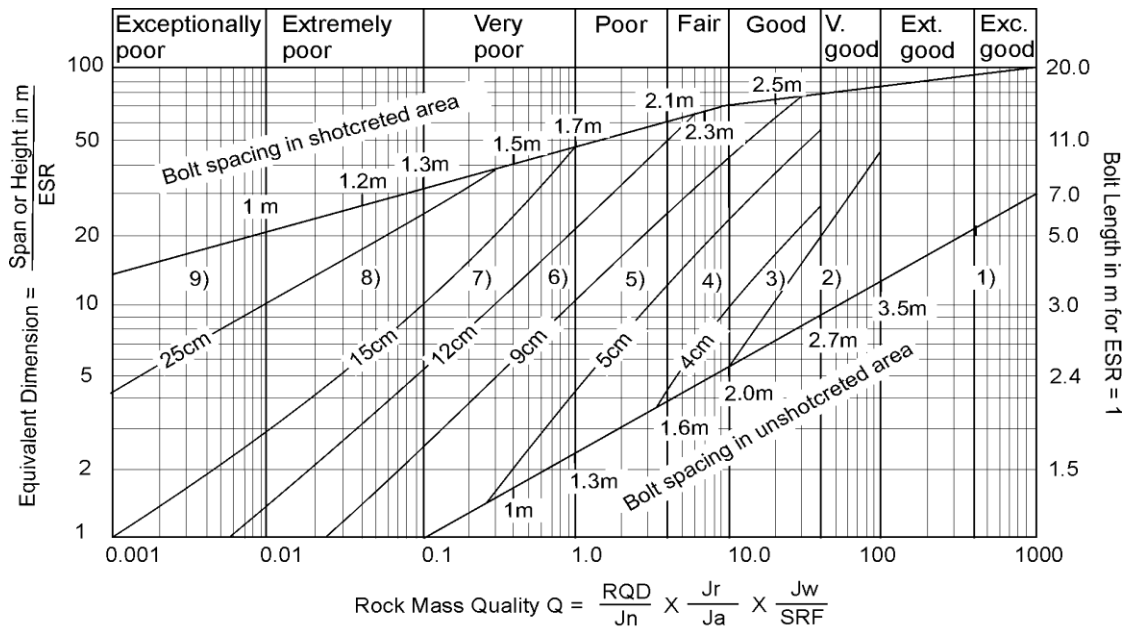

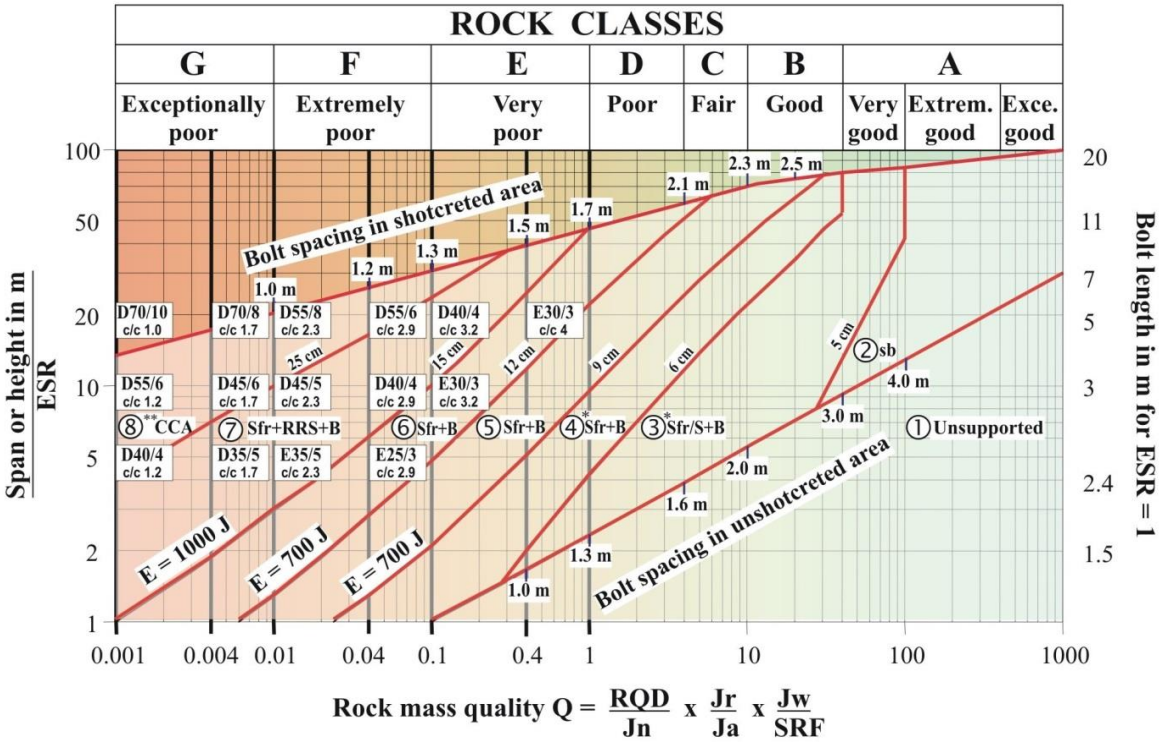

REINFORCEMENT CATEGORIES

1) Unsupported
2) Spot bolting, **sb**
3) Systematic bolting, and unreinforced or fibre reinforced shotcrete, 5-6 cm), **Sfr/B+S**
4) Fibre reinforced shotcrete and bolting, 6-9 cm, **Sfr+B**
5) Fibre reinforced shotcrete and bolting, 9-12 cm, **Sfr (E700) +B**
6) Fibre reinforced shotcrete and bolting, 12-15 cm, **Sfr (E700) +B**
7) Fibre reinforced shotcrete > 15 cm + reinforced ribs of shotcrete and bolting, **Sfr (E1000) +RRS+B**
8) Cast concrete lining, **CCA** or **Sfr (E1000) +RRS+B**

The bolts are 20 or 25 mm in diameter

E) Energy absorbtion in fibre reinforced shotcrete at 25 mm bending during plate testing

D45/6 c/c 1.7 = RRS with totally 6 reinforcement bars in double layer in 45 cm thick ribs with centre to centre (c/c) spacing 1.7 m. Each box corresponds to Q-values on the left hand side of the box

*) Up to 10 cm in large spans
) Or **Sfr+RRS+B

Figure 37a and b. Q-support charts dating from 1993 and 2007. Note the specification of RRS (rib reinforced shotcrete for exceptionally difficult (fault-zone) conditions. Today a minimum 5 cm of S(fr) is suggested for better curing/safety. The charts were first published by Grimstad and Barton, 1993 and by Grimstad, 2007.

7 AN UPDATE ON Q-SUPPORT CHARTS

With the present conference date of 2014 representing a 40-years anniversary since Q-system development, Barton and Grimstad, 2014 have recently produced an extensive and extensively-illustrated documentation of the recommended use of the Q-system, with numerous core- and tunnel-logged examples, and an extensive discussion of support and reinforcement principles. The article also documents important parametric linkages to Q and Q_c.

On the subject of support S(fr) and bolt reinforcement (B) for tunnels and mine roadways, Figures 37a and b should be consulted. It will be noticed that there are some minor adjustments to minimum shotcrete thickness, and details of RRS are given. This is the most secure way to come through fault zones compared to steel sets, unless there is too much water even for the more easily drained separated ribs (arches) of S(fr). As shown in Figure 38 (a to d), the key difference to 'standard methods' is that the ribs of shotcrete are bolted and rebar-reinforced, to minimize the loosening usually associated with use of steel sets, which allow too much deformation.

Note that each 'box' in Figure 37b contains a letter 'D' (double) or a letter 'E' (single) concerning the number of layers of reinforcing bars. Following the 'D' or 'E' the 'boxes' show maximum (ridge) thickness in cm (range 30 to 70 cm), and the number of bars in each layer (3 up to 10). The second line in each 'box' shows the c/c spacing of each S(fr) rib (range 4m down to 1m). The 'boxes' are positioned in the Q-support diagram such that the left side corresponds to the relevant Q-value (range 0.4 down to 0.001). Note energy absorption classes E=1000 Joules (for highest tolerance of deformation), 700 Joules, and 500 Joules in the remainder (for when there is less expected deformation). In general an S(fr) rib is applied first, to form a smoother foundation for the rebars. Shotcrete without fibre is used to cover the bars to avoid rebound of fibres.

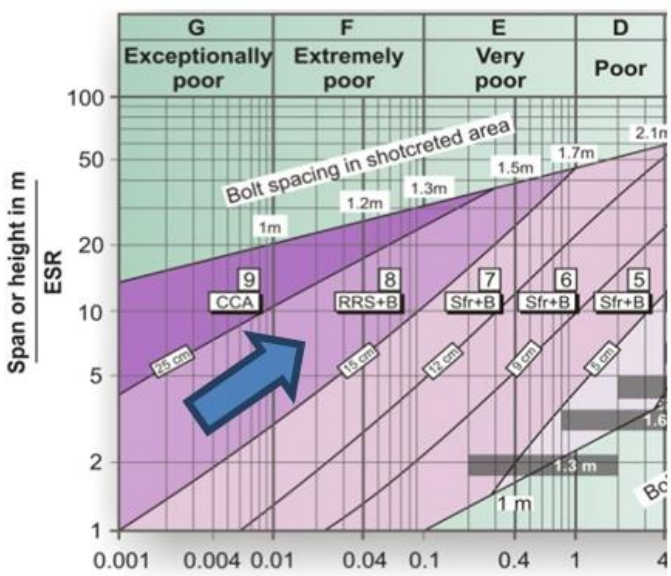

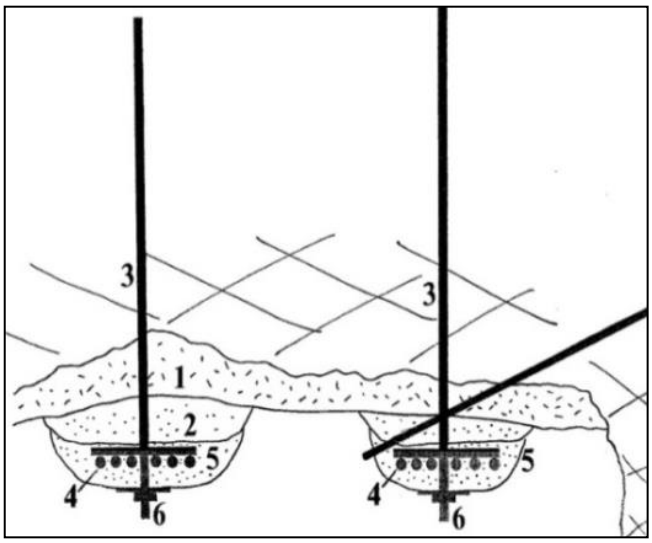

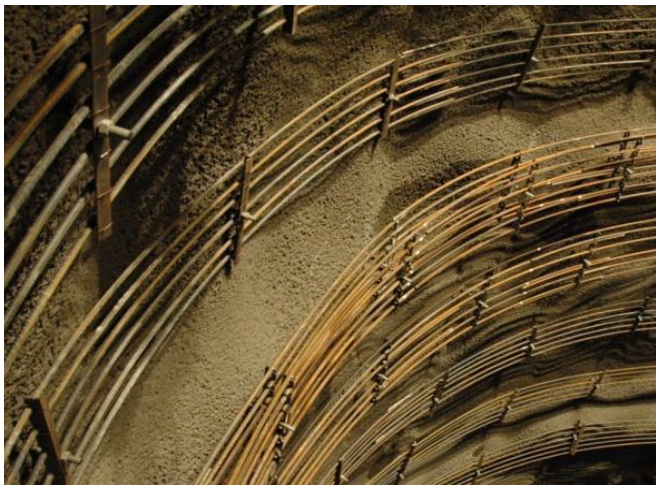

Figure 38 a, b, c and d. Some details which illustrate the principle of rib reinforced shotcrete arches RRS, which is an important component of the Q-system recommendations for stabilizing very poor rock mass conditions. The top photograph is from an LNS lecture published by NFF, the design sketch is from Barton 1996, the blue arrow shows in which part of the Q-chart the RRS special support-and-reinforcement measure is 'located'. The photograph of a completed RRS treatment is from one side of the 28 m span National Theater station in downtown Oslo, prior to pillar removal beneath only 5m of rock cover and 15m of sand and clay. Final concrete lining followed the RRS for obvious architectural reasons. Of course if access ramps to mines or 'permanent' mine roadways have to penetrate fault zones, the RRS can remain as final lining.

8 OVERBREAK AND STOPING WITH Q

The writer has worked mainly in civil engineering projects. Nevertheless on occasion there has been the opportunity to apply 'civil engineering' methods to mining problems. The case shown in Figure 39, was sketched from over-break situations in long-hole drilling tunnels in the LKAB Oscar Project, and is combined with one of the first applications of Q-histogram logging (in 1987). This case later became one of the sources for estimating over-break (and 'natural' caving) using the limiting ratio Jn/Jr ≥ 6.

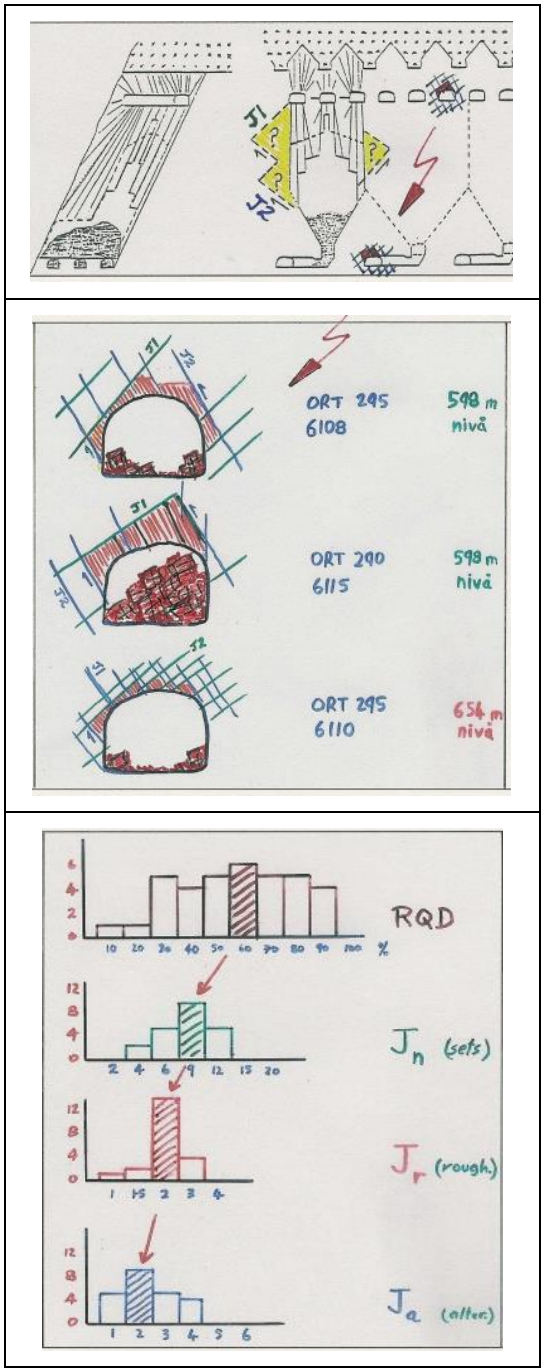

Figure 39. Observations of excessive over-break in some of the long-hole drilling tunnels, prior to stope development. Joint sets J1 and J2 had adverse *Jr/Ja* ratios in some cases (see outliers in the histograms). However it was the adverse ratios of *Jn/Jr* that were of most importance. Jn/Jr ≥ 6 meant over-break.

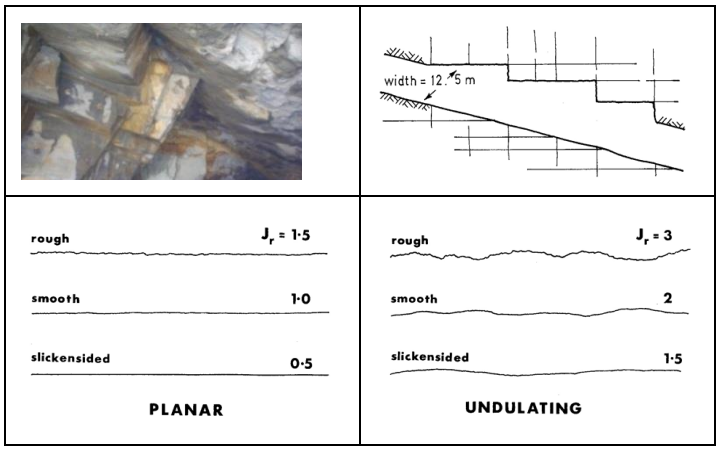

Figure 40. Even with Jn = 9 (three sets), a high enough value of Jr (2 or 3) may prevent over-break from occurring.

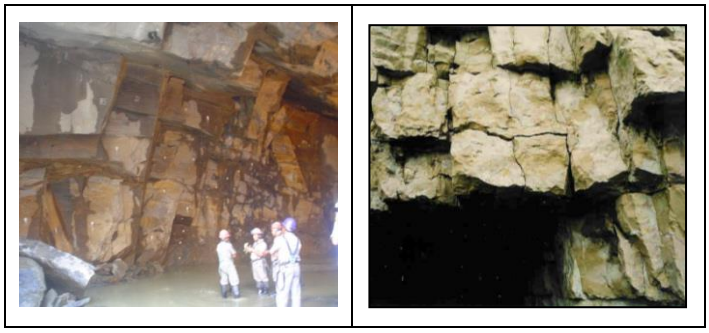

Figure 41. Examples left: of Jn/Jr = 9/(1-1.5), and right: Jn/Jr = 9/3. The two blocks at the entrance to a shallow room-and-pillar limestone mine have remained there for > 120 years.

Remarkably, this ratio of Jn/Jr applies to a wide range of Jn values (2, 3, 4, 6, 9, 12 and 15) and to a wide range of Jr values (1, 1.5, 2, 3, 4), using 'logical-thought' models – which could be confirmed with 3DEC. It therefore becomes a useful tool for assessing whether a contractor has blasted 'carelessly', or whether the over- break is inevitable, unless artificially short rounds were blasted, thereby compromising tunnel (or mine roadway / access ramp) production. (The record mine access speed: 5.8km in 54 weeks, with 174 m in best week: coal measure rock in Svalbard: contractor Norwegian LNS).

During a Q-related and high-stress course in Australia in 2006, the writer proposed the importance of Figures 39 and 40 to the potential for block-caving to the mostly mining-engaged participants. It was on this occasion that Dr. Frazer of CSIRO presented his 'Q-parameter ratio' studies in the subsequent discussion. Two of his figures are reproduced as a priv. comm. contribution in Figure 42. From memory of this occasion, Frazer had used stope characterization case records from the studies of Potvin, 1988, who had followed and modified the Mathews et al. Q'-based *stability graph methods* of the mid-eighties, during his work in Canadian mines. Following this well-documented study, the writer suggested in a mining workshop in Vancouver, the importance of Jn/Jr ≥ 6 on over-break and caving potential (Barton, 2007b). On this occasion the following was written:

It is quite likely that, whatever the overall Q-value at a given (potential) block-caving locality in an orebody, the actual combination J_n/J_r will need to be ≥6, for successful caving: e.g. 6/1, 9/1.5, 12/2 as feasible combinations of J_n/J_r, while such combinations as 9/3 might prove to be too dilatant. Even four joint sets (Jn = 15) with too high J_r (such as 3) would probably prejudice caving due to the strong dilation, and need for a lot of long-hole drilling and blasting. Significantly this last ratio (15/3 = 5) is also < 6.

With this useful introduction to the value of individual Q-parameters, thanks to the work of Frazer, it is an appropriate point for introducing the last topic of this paper: characterization of stope stability using the 'modified stability graph' method. This must necessarily be a brief commentary.

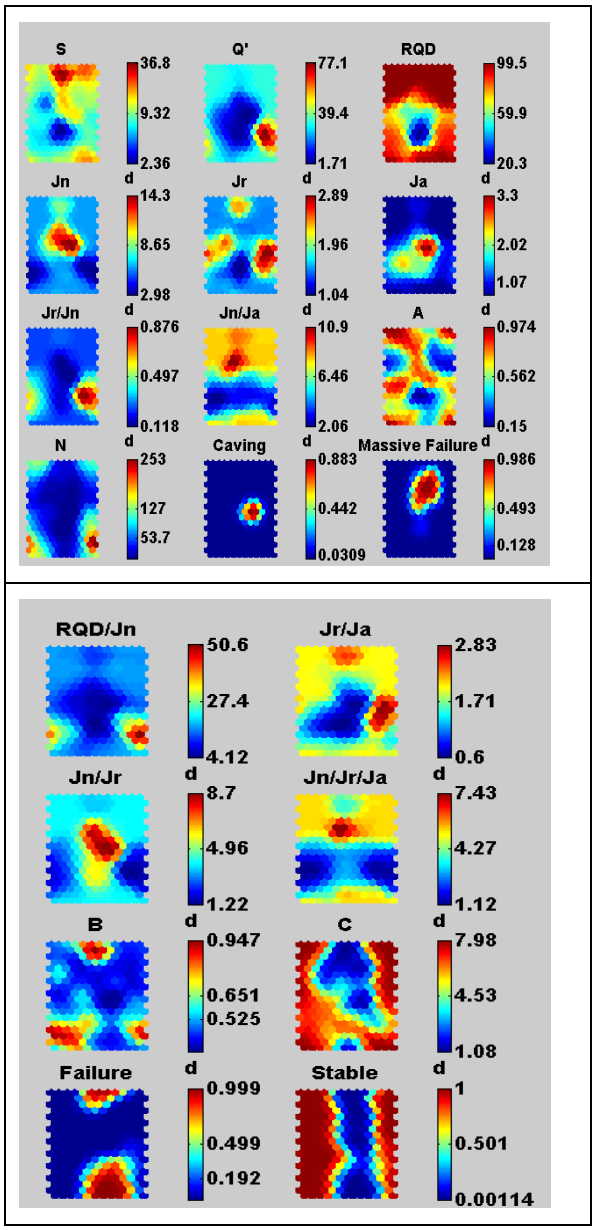

Figure 42. An original way to examine the influence of different Q-parameters (and their combination), on the possibility of caving or massive failure. (Pers. comm. Frazer, CSIRO, 2006). Note the closeness to the 'caving position' of Jn along, Ja alone and Jn/Jr.

It may be observed that the combination Jn/Jr/Ja does not work well. In fact it would be expected that (Jn/Jr) x Ja would be better. Note that the Jn/Jr (coloured) rating of probably 6 to 9 produces, as expected from prior discussion, the closest match to the 'caving position'.

8.1 *Stability Graph Factor N' starts with Q'*

The Stability Graph method was originally conceived by the Canadian Golders company, in Matthews et al., 1981, and later improved and modified to the stability number (N') (Potvin, 1988). Only the first two quotients RQD/Jn and Jr/Ja, which represent 'relative block size' and 'inter-block shear strength' are utilized in this method, and these of course are not by themselves sufficient descriptions of the degree of instability (Barton, 1999, 2002) when Jw and SRF are each set to 1.0. The possible presence of water (i.e. in sub-valley ore-bodies) and of faults or adverse stress/strength (both too high or too low) also needs to be included, at least when these are present. (The writer recalls the original difficulty of matching support needs when using only four or five of the original Q-parameters). As a result of these 'selected limitations', Q' (or Q-prime) is multiplied by three additional factors to obtain the Stability Index N' as follows (see Figure 43): N' = Q' x A x B x C. The values of A, B, and C relate to allowance for UCS/stress (similar to SRF), allowance for orientation of principal jointing, and allowance for failure mode, respectively.

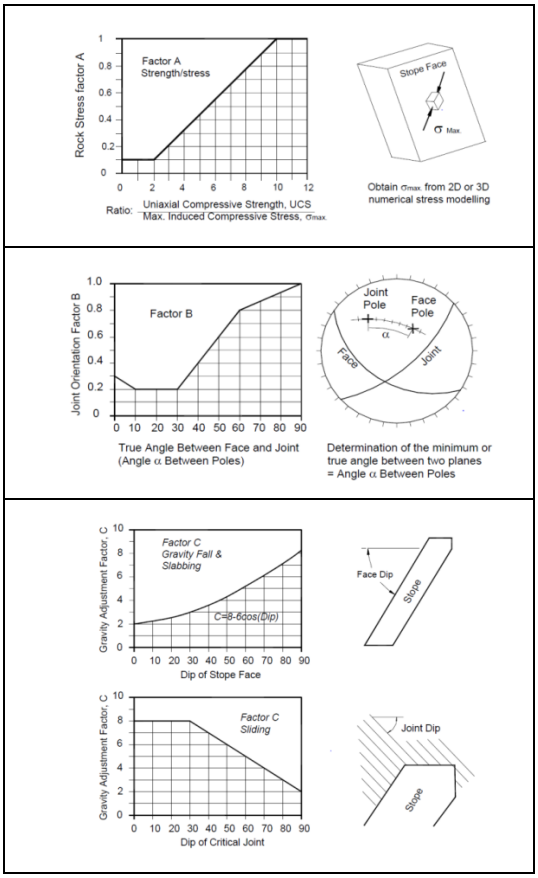

Figure 43. Diagrams to explain how to estimate Stability Graph Factors A, B and C. After Potvin (1988), reproduced second-hand from Huchinson and Diederichs (1996).The 'span' (width or diameter) as used in the Q-system, and the 'span from nearest support' as used in RMR, are replaced by the hydraulic radius, or area divided by perimeter, as commonly used in hydraulics, e.g. HR = XY/(2X + 2Y).

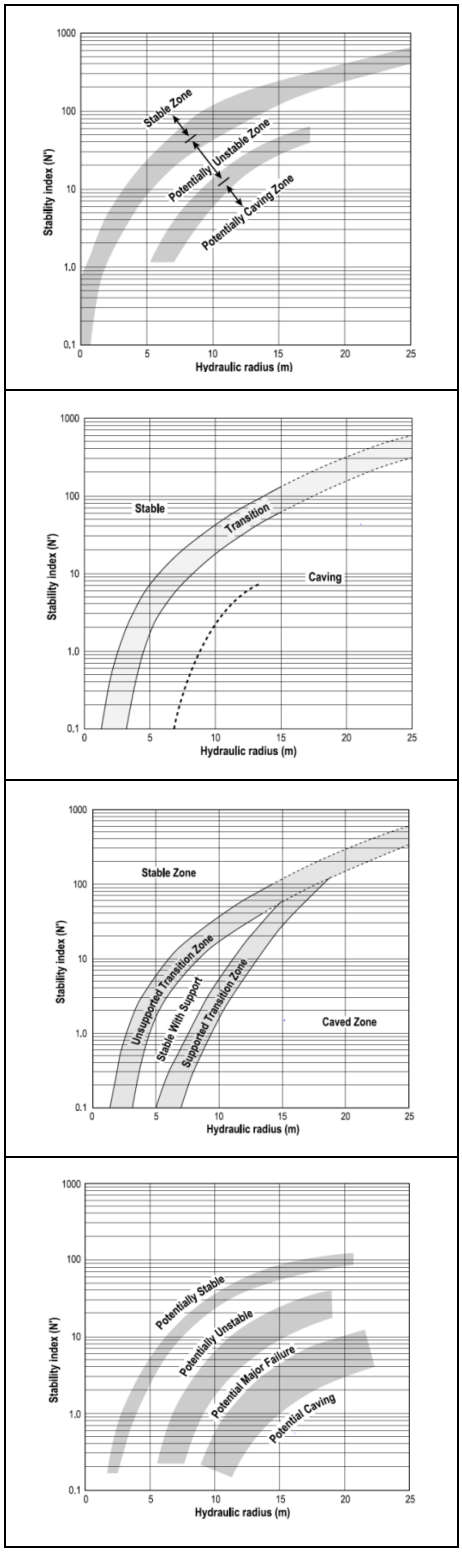

Figure 44 a, b, c and d. Stability index (N') versus the stope hydraulic radius. Various authors, from top: Mathews et al. (1981), Potvin (1988), Nickson (1992) and Stewart and Forsyth (1993). The specific graphic source of these figures was Potvin and Hadjigeorgiou (2001), as quoted by Capes (2009).

The four graphs (Figure 44 a, b, c and d) of stability number N' versus hydraulic radius (stope face-area divided by perimeter) show some mutual differences, reflecting the different authors different sets of case records, for instance weaker ore bodies, hard, narrow, steeply dipping etc. For example, Stewart and Forsyth (1993) emphasized that the (slightly earlier) versions of the graphs had very little data from mines with very weak or poor quality rock masses. Most of the case histories were from steeply dipping and strong ore bodies. The various 'variation-on-a-theme' methods have been reviewed by Potvin and Hadjigeorgiou (2001), and more recently by Capes (2009), from whom Figures 43 and 44 were reproduced.

A limited number of permanently unsupported civil engineering excavations (tunnels and caverns) from the Barton et al. (1974) data base, with Q-parameter analysis described in Barton (1976 b) are reproduced in Figure 44 b. These, together with the inclined ESR lines in Figure 44 c, help to visualize the different degrees of conservatism in civil engineering. Note that the ESR = 1.6 line is closest to the 'envelope' drawn in the central diagram. This is too conservative for temporary-stope mining use, as seen from Table 4 ESR values.

The four added 'cubes' in Figure 44 show the relative conservatism of civil works compared to mine stopes, which of course are designed to be temporary. The differences are not surprising in view of the design for 'permanency' in the world of civil construction in rock. The red curve corresponds to ESR (see Table 4) of about 4, a 'logical choice' within the 2 to 5 range of ESR for temporary mine openings suggested a long time ago (1974).

When conducting a short review in this field of 'stability graph' methods, the writer noticed some adverse practices on occasion, when viewing mining data concerning Q'. For instance, it is unfortunately not uncommon to see *only RQD* being varied, when Q' data is supposed to be used for stope categorization, using the 'modified Mathews' N and N' method.

8.2 Dilution or ELOS concept in mining

Recent research aimed at quantifying the dilution (or average over-break) in mining stopes were described by Capes (2009), who added considerably to the published data base. Some of his results will be reproduced here. Capes had published in the mining industry since 2005, and his dilution studies were part of his 2009 Ph.D., using several years' experience in Canadian, Australian and Kazakstan mines. Dilution, normally from the hanging-wall of a stope, though not exclusively, is basically large-scale over-break, caused by for instance, unfavourable ratios of

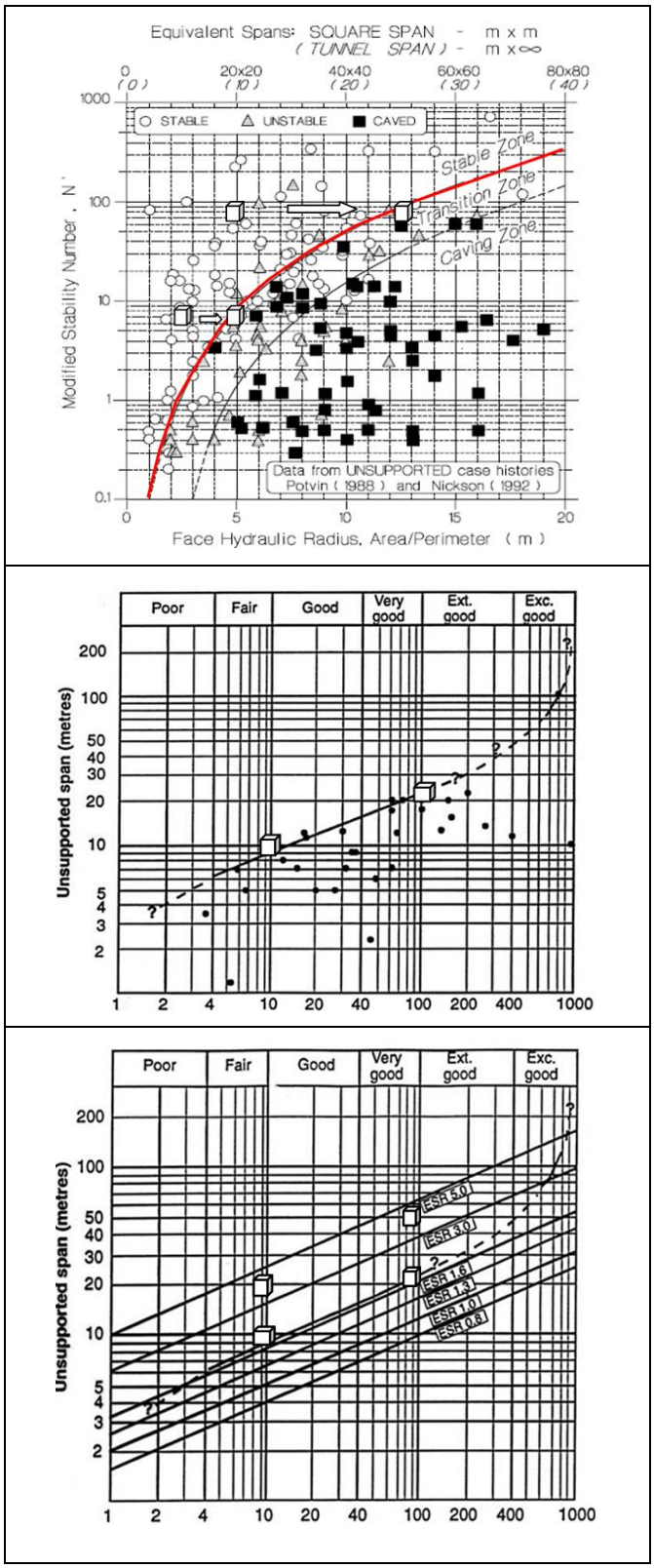

Figure 45. Top: The Potvin (1988) and Nickson (1992) combined data base of unsupported case records. Note helpful addition of (a more familiar) square span or tunnel span dimension in the top of the figure. Centre: Q-system permanently unsupported cases, and Bottom: the meaning the ESR lines, demonstrating the different degrees of conservatism. (Barton, 1976 b).The 'cubes' showing 10 m increasing to 20 m, and 20 m increasing to 50 m span (approx.) in order to reach the red envelope in the top diagram, are shown in equivalent positions in the SPAN versus Q (not Q') lines-of-equal ESR shown in the lower two diagrams.

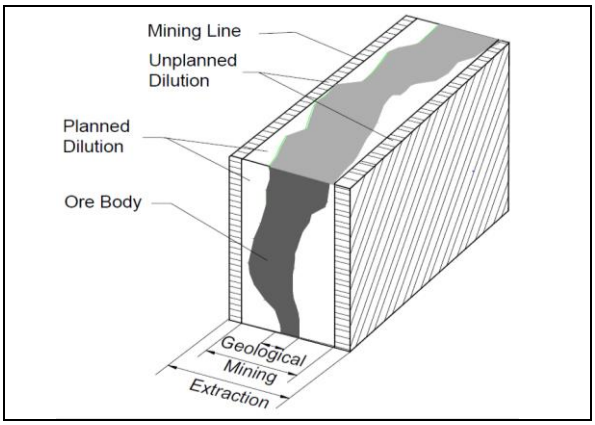

Figure 46. A simple definition of (average) dilution, beyond the planned and inevitable dilution. The figure is based on Scoble and Moss (1995), but was reproduced from Capes (2009).

Jn/Jr, as discussed earlier in this section. For covenience of volume estimation, it is averaged over the wall areas of the stopes, as simply illustrated in Figure 46. It is a volume of rock that has to be added to the amount needed to mine the ore. Clark and Pakalnis (1997) defined the factor ELOS (Equivalent Linear Overbreak\Slough) in an attempt approach to quantify overbreak regardless of stope width. ELOS is the volume of the rock failed from the stope hanging wall (HW) divided by the HW area which creates an average depth of failure over the HW surface.

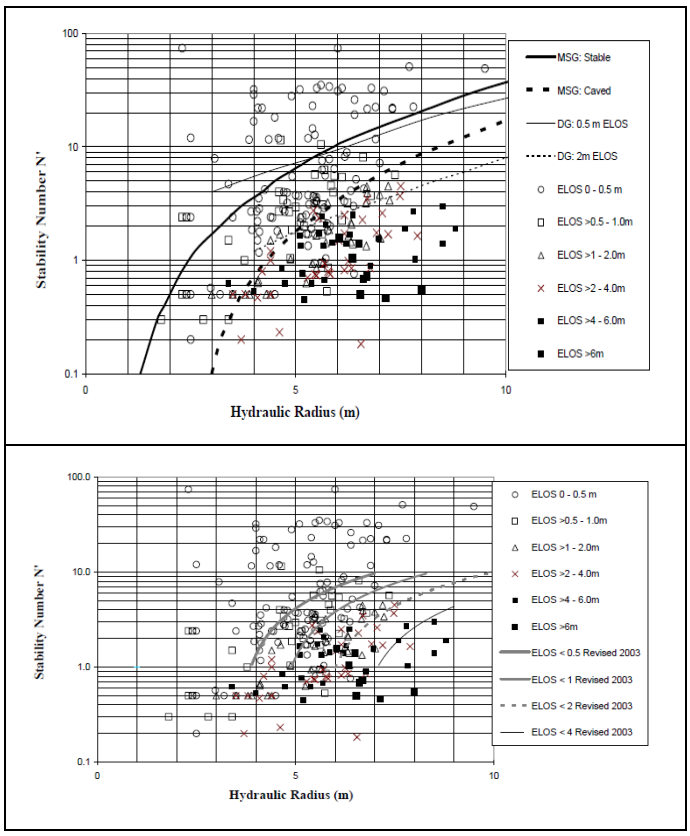

Figure 47. The 255 cases assembled by Capes (2009), showing: a) the stable and caved modified Stability Graph curves, and b) ELOS Dilution Graph curve.

It is clear that 'good quality' rock mass data related to stoping conditions is not very relevant to faulting and brecciation, as may be encountered as part of the ore-body rock masses. A fault can change the stresses in the stope hanging-wall, causing an increase in the zone of relaxation. Obviously there will also be a decrease in rock mass strength due to the increased fracturing and clay-coatings/fillings near the fault planes. In addition the fault, being a continuous feature, may form a key side of a kinematic failure surface, meaning locally deeper dilution/over-break. In many ways the selected 'removal' of SRF (related to faults *and* stress/strength ratios, i.e. SRF =1) when electing to use 'only' Q' seems to the writer not to have been a wholly logical move. After all, SRF *is* usually 1.0, but elevated SRF causing lower Q values, does seem to be needed when ore-bodies have faulted boundaries or interiors.

Weak-rock-mass data from five mines in Nevada (47 cases), were collected by Brady et al. (2005). Weak rock masses were defined by these authors as having a rock mass rating RMR of less than 45 and/or a rock mass quality rating (Q) under 1.0, meaning that there should be applicability to the more jointed/faulted/brecciated parts of such ore-bodies. Brady et al. (2005) made the observation that the classical design curves (ELOS) seem to be inaccurate at low N' and hydraulic radius values. They considered that if hydraulic radius was kept below 3.5 m in a weak rock mass, the ELOS value should remain under 1 m. They considered that a hydraulic radius under 3 m would not result in ELOS values much greater than 1m.

9. CONCLUSIONS

1. This paper started with some detailed consideration of the non-linearity of shear strength envelopes, both for intact rock, rock joints, and rock dump materials. This is nothing new: in fact it is 40 years old. Nevertheless a remarkable number of practitioners both in mining and petroleum engineering continue to use linear Mohr-Coulomb. A superior non-linear strength criterion now exists thanks to Singh et al., 2011.

2. It was suggested long ago (Müller, 1966) that breakage of cohesion and the remaining friction are in many ways separate entities. A small number of researches and consultants have so far adopted the 'c then σ_n tan φ' approach (degrading cohesion, while mobilizing friction). Greater realism results.

3. The shear failure of rock masses is a strain-and-process dependent event, and subsequently a displacement-and-process dependent event. Intact rock bridges, block corners and similar 'hindrances' break first at smallest strain. The high JRC, high JCS and high φ_r (= φ_b) fresh fracture surfaces are then 'immediately' mobilized, followed by the lower JRC, JCS and φ_r dominant joint sets, and eventual filled discontinuities or faults.

4. It makes no sense to *add* c and σ_n tan φ. The GSI-based Hoek-Brown criterion is convenient, but it is not providing the shear strength actually likely to be available or operating. The excessively complex equations also make it very opaque to changes of input data. So-called 'plastic zones' have been proved to be exaggerated when combined with continuum modelling using GSI and Hoek-Brown.

5. The deformation modulus of rock masses required for numerical modelling can be obtained via the Q-logging. It is linked with seismic velocity which is also stress or depth dependent. A depth or stress dependent modulus is required when performing modelling, especially if significant depth variation is involved.

6. It is useful to utilize empirical formulæ for checking modelled deformation. It is too easy to assume and model rock excavations with over-continuous jointing in UDEC, and thereby exaggerate the predicted deformations, which may be only one tenth as large when the rock excavation is actually constructed.

7. Over-break, and important indicators for block-cavability are found in the ratio of Jn/Jr. The logic applies over the full range of Jn values and Jr values. Over-break is inevitable with Jn/Jr $\geq$ 6, unless artificially short advances are demanded from the tunnel or mine-roadway contractor. The Jn/Jr ratio will also help to determine the level of energy required to initiate and maintain caving.

8. The modified stability graph method is built on the 'core description' of the rock mass and ore-body condition, using Q'= RQD/Jn x Jr/Ja. It is important that all four parameters are evaluated not just RQD, as seen sometimes in stope assessment work.

9. The obvious need for factor A to 'compensate' for the removal of SRF concerning the stress/strength ratio, leads one to also consider the wisdom of earlier developers who put Jw = 1and SRF = 1. What about an orebody beneath a deep river valley with a dominance of faulting and brecciation?

10. There is insufficient allowance for water and faulting because these facilities were removed during unilateral truncation of the Q-value. The most typical condition may well be Jw =1 and SRF = 1, but when other values are needed they are now 'unavailable'. This is unnecessary.

10. REFFERENCES

Bakhtar, K. & Barton, N. 1984. Large scale static and dynamic friction experiments. *Proc. 25th US Rock Mechanics Symp.* Northwestern Univ., Illinois.

Bandis, S., Lumsden, A. & Barton, N. 1981. Experimental studies of scale effects on the shear behaviour of rock joints. *Int. J. of Rock Mech. Min. Sci. and Geomech. Abstr*. 18, 1-21.

Barton, N. 1971. *A model study of the behaviour of steep excavated rock slopes. Ph.D. Thesis*, Univ. of London.

Barton, N. 1973. Review of a new shear strength criterion for rock joints, *Engineering Geology*, Elsevier, Amsterdam, 7, 287-332.

Barton, N., Lien, R. & Lunde, J. 1974. Engineering classification of rock masses for the design of tunnel support. . *Rock Mechanics.* 6: 4: 189-236.

Barton, N. 1976 a. The shear strength of rock and rock joints. I*nt. J. Rock Mech. Min. Sci. and Geomech. Abstr*., 13, 9: 255-279.

Barton, N. 1976 b. Unsupported underground openings. Rock Mechanics Discussion Meeting, Befo, Swedish Rock Mechanics Research Foundation, Stockholm, pp. 61-94.

Barton, N. & Choubey, V. 1977. The shear strength of rock joints in theory and practice. *Rock Mechanics*
1/2:1-54. Springer.

Barton, N. 1981. Shear strength investigations for surface mining. 3rd Int. Conf. on Stability in Surface Mining, AIME, Vancouver, 7: 171-192.

Barton, N. Modelling rock joint behaviour from in situ block tests: Implications for nuclear waste repository design. Office of Nuclear Waste Isolation, Columbus, OH, 96 p., ONWI-308, September 1982.

Barton N, Kjærnsli B. Shear strength of rockfill. J. of the Geotech. Eng. Div., 1981, 107 (GT7): 873–891.

Barton, N., Bandis, S. & Bakhtar, K. 1985. Strength, deformation and conductivity coupling of rock joints. *Int. J. Rock Mech. & Min. Sci. & Geomech. Abstr*. 22: 3: 121-140.

Barton, N. 1986. Deformation phenomena in jointed rock. 8th Laurits Bjerrum Memorial Lecture, Oslo. *Geotechnique,* 36: 2: 147-167.

Barton, N. 1990. Scale effects or sampling bias? Closing lecture. *Proc. of 1st International Workshop on Scale Effects in Rock Masses,* Loen, Norway. Balkema.

Barton N, By T L, Chryssanthakis P, Tunbridge L, Kristiansen J, Løset F, Bhasin R K, Westerdahl H, Vik G. Predicted and measured performance of the 62 m span Norwegian Olympic Ice Hockey Cavern at Gjøvik. Int. J. Rock Mech. Min. Sci. & Geomech. Abstr., 1994, 31 (6): 617–641

Barton, N. & Grimstad, E. 1994. The Q-system following twenty years of application in NMT support selection. 43rd Geomechanic Colloquy, Salzburg. Felsbau, 6/94. pp. 428-436

.Barton, N. 1996. Investigation, design and support of major road tunnels in jointed rock using NMT principles. Keynote Lecture, IX Australian Tunnelling Conf. Sydney, 145-159.

Barton, N. 1999. General report concerning some 20th Century lessons and 21st Century challenges in applied rock mechanics, safety and control of the environment. Proc. of 9th ISRM Congress, Paris, 3: 1659-1679, Balkema, Netherlands.

Barton N. Some new Q-value correlations to assist in site characterization and tunnel design. Int. J. Rock Mech. & Min. Sci., 2002, 39 (2):185–216.

Barton, N. 2006. *Rock Quality, Seismic Velocity, Attenuation and Anisotropy.* Taylor & Francis, 729p.

Barton, N. 2007a. Near-surface gradients of rock quality, deformation modulus, Vp and Qp to 1km depth. First Break, *EAGE,*October, 2007, Vol. 25, 53-60.

Barton. N. 2007b. Rock mass characterization for excavations in mining and civil engineering. Proc. of *Int. Workshop on Rock Mass Classification in Mining*, Vancouver.

Barton, N. 2008. Shear strength of rockfill, interfaces and rock joints and their points of contact in rock dump design. Keynote lecture, Workshop on Rock Dumps for Mining, Perth, p. 3-17.

Barton, N. and S.K. Pandey, 2011. Numerical modelling of two stoping methods in two Indian mines using degradation of c and mobilization of φ based on Q-parameters. *Int. J. Rock Mech. & Min. Sci.,* 48,7: 1095-1112.

Barton N. 2011. From empiricism, through theory, to problem solving in rock engineering. ISRM Cong., Beijing. 6th Müller Lecture. Proceedings, Harmonising Rock Engineering and the Environment, (Qian & Zhou ed), Beijing Taylor & Francis, (1):3-14.

Barton, N. 2013. Shear strength criteria for rock, rock joints, rockfill and rock masses: problems and some solutions. J. of Rock Mech. & Geotech. Engr., Wuhan, Elsevier 5(2013) 249-261.

Barton, N. 2014. Non-linear behaviour for naturally fractured carbonates and frac-stimulated gas-shales. First Break, EAGE, the Netherlands.

Barton, N. and E. Grimstad, 2014. Tunnel and cavern support selection in Norway, based on rock mass classification with the Q-system. Norwegian Tunnelling Society, NFF, Publ. 23. 39 p.

Barton, N. and E. Quadros, 2014. Gas-shale fracturing and fracture mobilization in shear: *Quo Vadis*? *Rock Mechanics for Natural Resources and Infrastructure. SBMR.* ISRM specialized conference, Goiana, Brazil, 12p.

Byerlee, J.D. 1978. Friction in Rocks. *Journal of Pure and Applied Geophysics,* 116, 615-626.

Capes, G.W. 2009. Open stope hanging-wall design based on general and detailed data collection in rock masses with unfavourable hanging-wall conditions. Dept. of Geological and Civil Engineering, Univ. of Saskatchewan, Ph.D.

Clark, L. and Pakalnis, R., 1997. An empirical design approach for estimating unplanned dilution from open stope hangingwalls and footwalls. CIM AGM, Vancouver.

Edelbro C. (2009). Numerical modelling of observed fallouts in hard rock masses using an instantaneous cohesion-

softening friction-hardening model. Tunnelling and Underground Space Tech. 2009, 24 (4):398–409.

Grimstad, E. & Barton, N. 1993. Updating of the Q-System for NMT. Proceedings of the International Symposium on Sprayed Concrete - Modern Use of Wet Mix Sprayed Concrete for Underground Support, Fagernes, 1993, (Eds Kompen, Opsahl and Berg. Norwegian Concrete Association, Oslo.

Grimstad, E. 2007, The Norwegian method of tunnelling – a challenge for support design. *XIV European Conference on Soil Machanics and Geotechnical Engineering.* Madrid.

Hajiabdolmajid,V., C. D. Martin and P. K. Kaiser,. Modelling brittle failure. *Proc. 4th North American Rock Mechanics Symposium, NARMS 2000* Seattle J. Girard, M. Liebman, C. Breeds and T. Doe (Eds), 991–998. Balkema.

Hudson, J.A., Jones, E.J.W. & New, B.M. 1980. P-wave velocity measurements in a machine-bored, chalk tunnel. *Q. J. Engng Geol.*, *13*: 33–43. Northern Ireland: The Geological Society.

Hutchinson, D.J. and Diederichs, M.S., 1996. Cable-bolting in underground mines. BiTech. Publishers Ltd.

Leps, T. M. 1970. Review of shearing strength of rockfill. *J. of Soil Mech. & Foundations Div.*, ASCE, Vol. 96, No. SM4, Proc. Paper 7394.

Mathews, K.E., Hoek, E., Wyllie, D., and Stewart, S.B., 1981. Prediction of stable excavation spans for mining below 1000 metres in hard rock, Canada: CANMET, Dept. of Energy,Mines and Resources.

Müller, L. 1966. The progressive failure in jointed media. *Proc. of ISRM Cong*., Lisbon, 3.74, 679-686.

Nickson, S.D., 1992. Cable support guidelines for underground hard rock mine operations. M.Sc. Thesis, Univ. of British Columbia, Canada.

Potvin, Y.,1988. Empirical open stope design in Canada, Ph.D. thesis. Univ. of British Colombia, Canada, 350p.

Potvin, Y., and Hadjigeorgiou, J., 2001. The stability graph method for open-stope design. IHustrulid WA, Bullock RL, editors. Underground mining methods: engineering fundamentals and international case studies. Littleton, Colo: Soc Mining Metall Explor; 2001, p513-519.

Scoble, M.J., Moss, A., 1994. Dilution in underground bulk mining: Implications for production management, mineral resource evaluation, methods and case histories, Geological Society Publication No. 79, pp. 95-108.

Shen, B. & Barton, N. 1997. The disturbed zone around tunnels in jointed rock masses. Technical Note, *Int. J. Rock Mech. Min*. Sci, 34: 1: 117-125.

Shen, B., O. Stephansson, and M. Rinnie, 2013. *Modelling Rock fracturing Processes – A Fracture Mechanics Approach Using FRACOD.* Springer, 173p.

Singh, M., Raj, A. and B. Singh, 2011. Modified Mohr-Coulomb criterion for non-linear triaxial and polyaxial strength of intact rocks. *Int. J. Rock Mech. Mining Sci.*, 48(4), 546-555.

Singh, M. and B. Singh, 2012. Modified Mohr–Coulomb criterion for non-linear triaxial and polyaxial strength of jointed rocks. Int. J. Rock Mech. & Min. Sci. 51: 43-52.

Stewart, S.B.V., and Forsyth W.W., 1995. The Mathews method for open stope design. CIM Bull. Vol.88 (992), 1995, pp. 45-53.

Sutton, D. 1998. Use of the Modified Stability Graph to predict stope instability and dilution at Rabbit Lake Mine, Saskatchewan, Univ. of Saskatchewan Design Project, Canada.